Advanced Grid-Tied Photovoltaic Micro-Inverter

Yuheng Lu

A thesis submitted in partial fulfilment
of the requirements for the degree of
Master of Engineering
in
Electrical and Computer Engineering
at the
University of Canterbury,
Christchurch, New Zealand.

2015

ABSTRACT

Along with the damaged environment and the emerging energy crisis, many problems have been caused by utilizing fossil fuels. Green energy, also known as renewable energy, has been trusted as a good alternative for the conventional energy resources and effort has been contributed in the development of modern green energy. Solar energy is one of the renewable energy resources. Owing to its advantages of being nearly unlimited, pollution free, noise free and relatively easy to maintain, photovoltaic (PV) systems have experienced a significant increase in the past few decades. In this thesis, a grid-tied solar micro inverter has been presented and several key technology issues on this PV system are investigated:

1. Maximum power point tracking (MPPT) strategies. Under changing atmospheric conditions, intensity of the sunlight irradiation and shading problems, the output of a solar panel varies non-linearly. MPPT techniques are designed to enable PV panels always operate at the optimal power point and produce maximum power. In this paper, different MPPT strategies are compared and analysed. An improved variable step-size P&O MPPT strategy is also proposed to compensate those drawbacks from conventional MPPT techniques. Simulation results are also given.

2. Control strategies of a single-phase grid-tied inverter. A deadbeat controller, named the OSAP control, is proposed for the inverter. This inverter is analysed into two states: stand-alone inverter and grid-tied inverter. In each state, the OSAP controller is applied to control the inverter. Some disadvantages are also shown for the OSAP controllers. An improved OSAP controller is then introduced to compensate these drawbacks. Simulation results are given to support the theory.

3. Experiment of this solar inverter. An interleaved boost converter is shown to implement the MPPT techniques. Experiments of the stand-alone inverter and grid-tied inverter are also conducted with the OSAP control strategies. The experiment of this PV system under some environmental changes are also conducted and the transient response is given.

Chapter 1 deals with the background introduction and literature review. A model of solar cell is introduced in Chapter 2 and the simulation model is also built to analysis the characteristics of solar panel output power. Several Maximum Power Point Tracking (MPPT) techniques are evaluated and an improved variable step-size MPPT technique is proposed to overcome the

disadvantages. In Chapter 3, a control strategy is developed for a grid-tied PV micro-inverter, which is called one-sampling-ahead-preview (OSAP) control. Firstly a full-bridge inverter is analysed. Two states of this inverter are introduced, one is the stand-alone inverter and the other is the grid-tied inverter. Mathematical and simulation model have been built for each inverter. Then an OSAP voltage controller is proposed for the stand-alone inverter and an OSAP current controller is proposed the grid-tied inverter. However, since OSAP controllers belong to the deadbeat control category, these exists a deadbeat response in the output. And another problem is that OSAP controllers highly depend on the inverters have accurate parameters for the components, which is not practical in real life. So an improved OSAP controller is introduced to solve these problems, which is the OSAP with a resonant controller. Simulation results are also given to support the theory. In Chapter 4, the experiment of this system has been shown and experimental results have been provided. Chapter 5 explains the conclusions and some developments need to be done in the future work.

ACKNOWLEDGEMENTS

First and foremost, I would like to express my sincere gratitude to my advisor Dr Alan Wood for his excellent guidance, caring, patience, and providing me with an excellent atmosphere for doing my research. I attribute the level of my Masters degree to his encouragement and effort and without him this thesis, too, would not have been completed or written. One simply could not wish for a better or friendlier supervisor. Also I want to thank Dr Keliang Zhou for helping me find an interesting research topic and offering sufficient effort to the new controller I utilized in this thesis.

My sincere thanks also goes to the technicians in the power electronics lab, and in particular, to Mr Edsel Villa. Without his guidance and his excellent practical experience in the industry, those problems during my experiment would not be solved. Besides, dozens of people have helped and taught me immensely at the university. Thank you to those who helped my project as staff and friends: Rabia Nazir, Patrick Chen, Alejandro Castellanos Escamilla, Zhiyang Jin, Diwakar Bhujel, Yanosh Irani, Xueshu Cao and Lance Frater. Thank you guys for all you have done for me.

Finally, the most important and the sincerest gratitude to my parents for their exceptional love to me and the whole family. Thanks for their encouragement through my life and the support for my studies oversees. I always believe, no matter what happens, they will never give up on me and always stand by me through the good times and bad.

CONTENTS

LIST OF FIGURES

LIST OF TABLES

Chapter 1

INTRODUCTION

1.1 BACKGROUND

Abundant and economic energy is the life blood of modern civilization [1]. With the increasing speed of global economic growth as well as the remarkable development in world industry, the fast rising demand for sustainable energy has put ever-increasing pressure on human society. Not only is humankind running low on easily obtainable fossil fuel resources, but the associated environmental impact of fossil fuel use is reaching crisis levels. In this case, green energy, also named renewable energy, is the best choice as an alternative resource for the world industry. Generally, the mainstream technologies applied in the green energy field can be classified as wind power, hydro-power, solar power, geothermal power and biomass power [2]. Along with the amazing innovations in the photovoltaic (PV) technology, solar power has attracted plenty of attention. Due to several reasons including the unlimited energy from the sun, the relatively high efficiency of modern PV system, the continuously dropping price of solar cells and the ease of implementation and maintenance of solar systems, the PV industry is taking more of a role in world power supply.

1.1.1 World Energy Crisis

Global energy demand was approximately 16TWh in 2012 and is expected to double in the next twenty years [3]. While innovations in power generation technology offer a great help to the energy production via traditional resources, a critical problem has emerged which can not be simply ignored or eliminated by advanced technology—the world energy crisis, especially in fossil fuels. Actually, the energy crisis or the oil crisis, is not a new concept. The world market experienced a crisis in the second half of the 1970s with a continuously increasing oil price. At that time, the economic issue was the most important factor and attention decreased when the oil price fell. Sustainability in terms of fossil fuel supply is often treated as short-term economic and political issues [4]. However, in 21st century, the second oil crisis is more thorny, and the

economy is not the only worrying factor. In fact, we now have concerns about the future of human society.

The world has experienced a huge increase in energy demand during the last 200 years. Fig. 1.1 gives the details about the significant rise of the global energy demand. It can be noticed that nowadays we consume over 10 times more energy than we did in 1820. Improved technologies and the fast growing population are mainly responsible for this huge increase. However, it is also clear that the majority of the energy resources that we rely on are not sustainable. Since crude oil is made over millions of years from an ancient biota, the overuse of oil means that we cannot depend solely on these resources for very much longer. Table 1.1 is based on the BP Statistical Review of World Energy 2010 that illustrates their estimate of the remaining energy resources over the world. According to this estimate, the most important energy resources—oil, could only last for 45 years, which means our current industry system will face a severe challenge by 2045. Besides the oil shortage, other energy resources (except solar power) can only support our economy for several decades; looking for alternative energy resources is imperative for all of us.

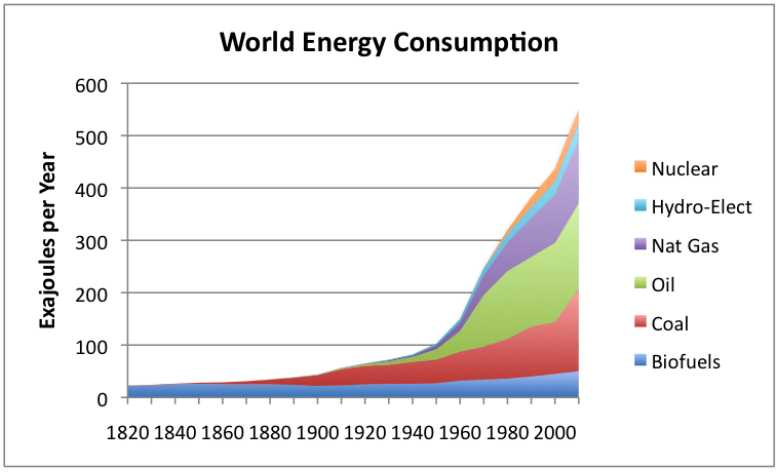

Figure 1.1: World energy consumption from 1800s to 2000s

Table 1.1: Estimation of the remaining energy resources all over the world

Oil	45 years
Coal	61 years
Natural Gas	230 years
Uranium	71 years
Solar	unlimited

*all the data are calculated from 2000

1.1.2 The Thrust For Renewable Energy

The other problem caused by burning fossil fuel is pollution, and the consequent environmental and climate change. Unfortunately, some of the pollution appears to be irreversible. During the 1980s and 1990s, most governments conducted a deregulation policy in their countries, which was treated as a positive way to encourage the efficient supply and use of energy [2]. An important attempt to deal with the energy problem and pollution globally was the Kyoto protocol in 1997. Despite that America and China, being the two largest polluting nations, were not involved, the Kyoto protocol indicated that more attention should be paid to this serious problem. Renewable resources, such as solar power and wind power, are being trusted as a replacement of conventional energy resources in the future. Considerable efforts have contributed to the fast growth of green energy in the last few years.

Prior to the development of coal in the mid 19th century, nearly all energy used by human society was renewable. Among the energy sources, hydro (in the form of flow of the river wheels) and wind (in the form of wind mills) have been used for centuries as sources of mechanical power, mainly for agriculture purposes [2]. However, nowadays when we talk about renewable energy, we are using these resources to generate electrical power. Green energy is defined as energy that comes from resources which are naturally replenished in a human timescale, including wind power, hydro power, solar energy, geothermal energy and bio energy. Fig. 1.2 comes from the World Bank Renewables 2015 Global Statues Report and it gives us a clear view of how important green energy is for human society. Despite fossil fuel still being responsible for about 78.4% of energy consumption all over the world, renewable resources now can shoulder as much as one-fifth of our energy needs. Looking forward to the future, indications are that the need to push in the direction of renewable energy is being taken seriously and there is a bright future for these technologies [2].

Abundant renewable energy is available for New Zealand compared to many other countries, and this has helped NZ achieve a high percentage of clean electricity utilized in the domestic grid. Among these, the large-scale renewable energy resources such as wind farms, geothermal, and hydro energy, have already played an important role in providing sufficient and reliable power for personal and business consumers [5]. New Zealand is proud to be one of the cleanest energy providers in the world, and around 40% of its primary energy is supplied by green energy resources [6]. Meanwhile, the NZ government has announced that New Zealand is aiming to be the first carbon neutral country by 2020. Fig. 1.3 shows research from the NZ government about the renewable energy consumption in 2011 and the projection up to 2030. By 2025, New Zealand has a target of 90% of all electricity generation coming from green energy resources [7].

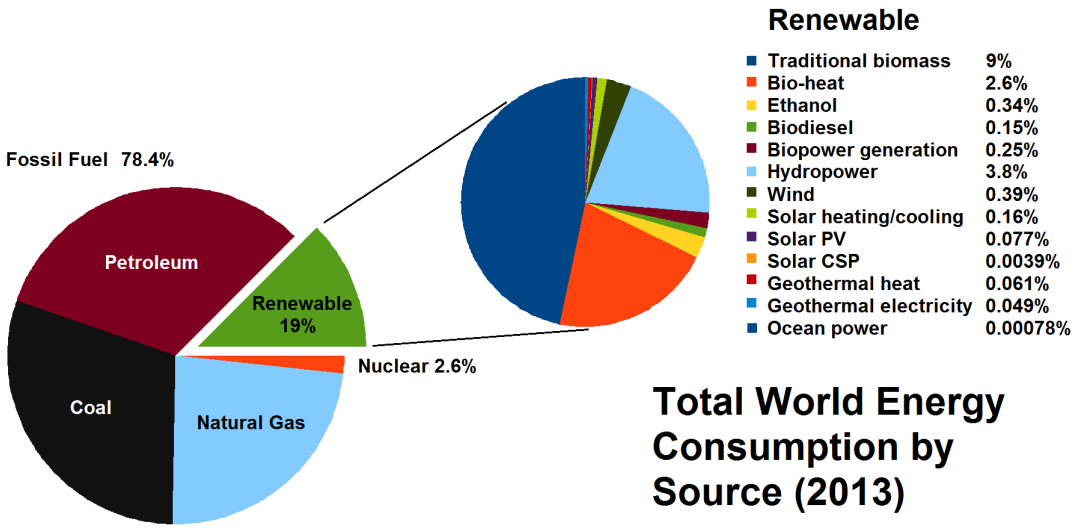

Figure 1.2: World energy consumption by source at 2013

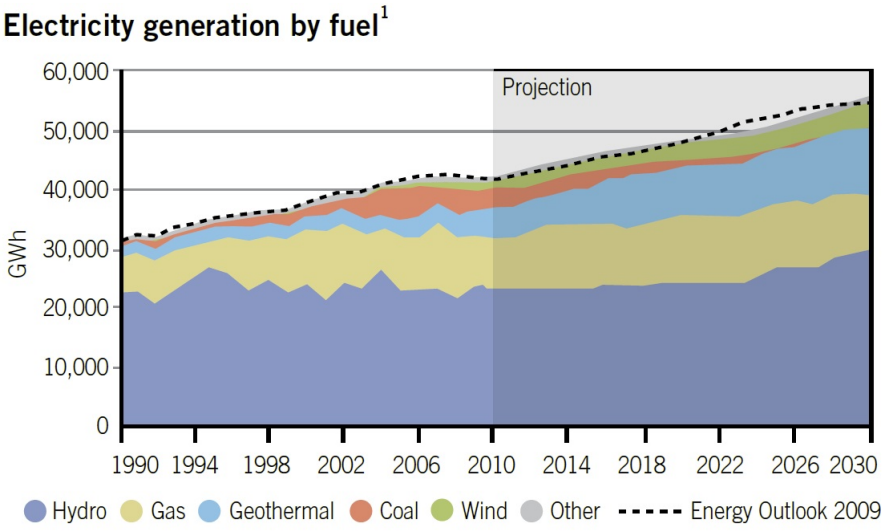

Figure 1.3: New Zealand Energy Strategy in 2011

1.2 PHOTOVOLTAIC SYSTEM AND DISTRIBUTED GENERATION

Among all of these renewable energy resources, the most abundant, sustainable energy source is the sun, which delivers over 150000 TW of power to Earth. Even though half of this power has been wasted before it reaches the earth surface and only a small fraction is practically available for electricity generation, the amount of power is more than enough to satisfy global energy demand. One of the greatest technological and scientific challenges facing us today is to develop efficient ways to collect, convert, store and utilize solar energy at affordable costs [3]. Basically, there are three ways to utilize the solar power—providing energy to grow biomass, collecting the heat from the sunlight in solar thermal systems or converting the solar irradiation into

electricity in PV systems. A PV system employs solar panels to supply usable electric power and these solar panels usually come with an inverter to transfer their output DC power into AC power and feed back to the customers in an electric power grid. PV technology is a new technology comparing with other renewable energy resources. PV systems have been used for fifty years in specific applications and have only been used as grid-connected systems for twenty years [8]. For now PV systems have not dominated the market as an affordable renewable energy resource, and account for only 0.077% of the world energy generation in 2013 (Fig. 1.2). The relatively high price and the inconvenience of no power supply at night are the main barriers to the widespread adoption of PV systems in the industry. However, the cost of PV cells has decreased steadily from US $20/W in 1990 to less than US $0.7/W in 2014 [3]. Along with the incredible innovations in semiconductor industry which can also benefit solar cells, we have confidence that PV industry has a bright future and it will take more of a role in electricity generation as a reliable and affordable green energy resource in the foreseeable future.

1.2.1 Classification of Solar Inverters

Several types of PV inverters are available in the market now. Fig. 1.4 illustrates that one method of classifying solar systems is based on the power rating. At the low power end is the micro-inverter system, which can process up to 300W per unit. The other two inverters (string inverters and multi-string inverters) actually share the same topology, which is named central-inverter topology. String inverters are usually at 1 kW to 10 kW power rating and are widely used in residential applications, while multiple-string inverters can process more power and are an important part of commercial solar plants.

Besides the power rating, another significant difference between micro inverters and central inverters is that every solar panel is controlled by an inverter and they form an independent module in the micro-inverter system, while in the central-inverter systems several solar panels are combined together as a PV string, all of these solar panels are controlled by only one single central inverter in the system. Central string inverters are currently the most cost-effective option available and they have more than 40 years development history [9]. However, micro inverters are rapidly gaining popularity, especially for residential solar applications. In fact, the micro inverter concept is not new to the market. The unpopularity of micro inverters is mainly due to the relatively high price. Nowadays, with the decreasing price of both solar panels and semiconductor equipment, more PV companies have raised funds and sharpened their marketing pitches to take on the conventional central inverter players [9]. The advantages that micro inverters have over central inverters are listed as follows:

1. High efficiency. One of the most important factors when designing a solar system is the efficiency. Before discussing the efficiency of solar systems, several facts have to be mentioned. Even though they generate DC power, solar cells have unique output characteristics whose output

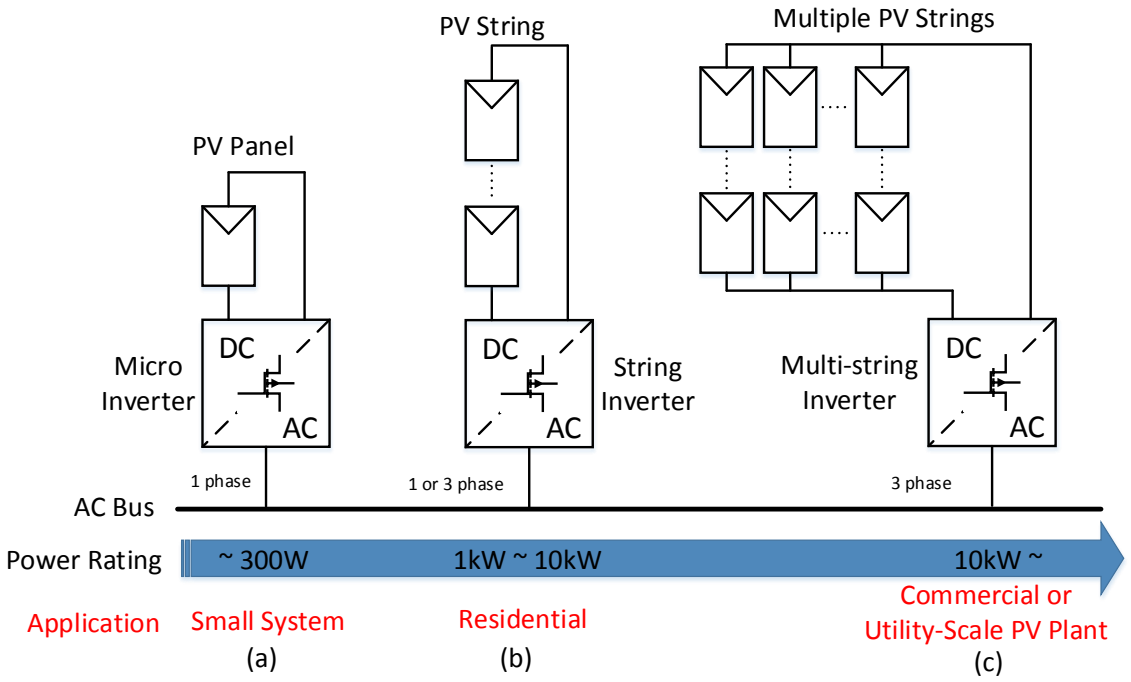

Figure 1.4: Grid-connected PV systems: (a) Micro inverter (b) String inverter (c) Multi-string inverter

is not constant and will change with the temperature and the sun shine. There is only point point that can make sure a solar panel is generating its maximum power according to the current condition. A technique is designed specifically for solar cells to guarantee the optimal output, which is called Maximum Power Point Tracking (MPPT). It is a well-known fact that shading is a practical problem that affects solar panel output power and consequently the efficiency of the whole system. This unpredictable and unpreventable problem is supposed to be solved by MPPT techniques. In central-inverter systems, since several PV panels are connected together and are controlled by the central inverter, if some of the panels are shaded and the others are not affected, it is hard for the MPPT controller to search the optimal point. By contrast, if each solar panel is controlled by its own inverter and these solar panels are independent of each other, even though some panels are affected by shading, the rest can still work fine. This is the idea of designing a micro inverter system. By this mechanism, the effectiveness of micro inverters can be much higher than central inverters.

2. Simplicity. A central inverter has to be carefully evaluated before designing, because when more panels are needed in the future, the central inverter may have to be redesigned for the new power demand. With micro inverters, things become much more convenient. Adding another micro inverter system does not have any influence on the existing one as they are independent. The simplicity and convenience of micro inverters makes them suitable for residential applications.

3. Safety. One fact is that the output current of a solar panel at the MPP is quite close to the

short-circuit current. If one panel has a short circuit, it is very difficult for the central inverter to detect this tiny change, compared with the large value of current handled by the central inverter when several PV panels are connected in parallel. The short-circuit problem is very dangerous for electrical systems, which can damage solar panels. By contrast, a micro inverter is monitoring only one panel in the system and has the ability to raise the alarm when a short circuit happens.

1.2.2 The Rising Concept of Distributed Generation

Distributed Generation (DG) is an important component of smart grid, a concept that replaces the existing model of one-way electricity supply from centralized generation plant to end consumers with an arrangement that allows for electricity to flow in optimal directions, depending on prevailing conditions. Distributed generation may allow passive electrical consumers to become more engaged and active participants in managing their own energy needs [5]. The rising concept of DG is derived from the emerging range of small-scale power resources available for residential applications and the requirements of power customers to have more active engagement in the power grid. Different from the conventional centralized power grid, DG allows power generation at the point of consumption, which means suitable power generators are installed at the customer sites and feed power to the grid when available. Technologies that suit small and medium size DG applications include internal combustion engines, gas turbines, micro-turbines, fuel cells and some renewable energy resources [10].

Indiscriminate application of individual distributed generators can cause unpredicted problems since DG is still a new concept for the industry. Another way to realize the emerging potential of DG is to take a system approach which combines the distributed generators and the connected loads as a subsystem or a microgrid [10]. In a microgrid, control of distributed generation no longer belongs to the central utilities and local control is available for power supply and disturbance elimination. This advantage ensures stable power supply to local customers during grid fault situation. Even though sufficient researches and tests have been conducted to prevent serious problems in modern power grid, some issues such as the power shortage still exist. The problem is worse for DG system, which is known as the islanding problem when the grid power supply is cut off. With the help of local controllers in the microgrid, no matter an intentional or a unpredictable islanding problem happens, the microgrid itself can be cut off from the utility immediately and power supply from DG system can be kept stable and safe for the local customers without harming the transmission grid's integrity. Along with the stable power supply, reducing the cost of generating and delivering power, reducing the transmission losses, utilizing the green energy and reducing the electricity price are all the benefits that can be enjoyed by both the customers and power companies.

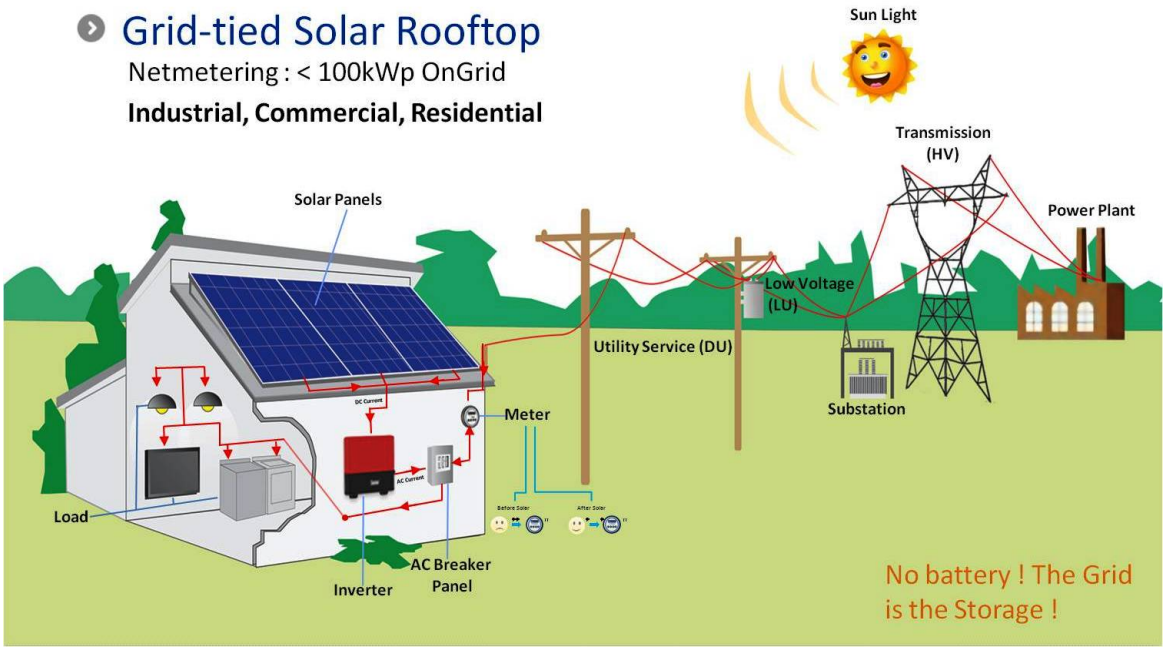

Figure 1.5: Example of a residential PV installation as DG system

1.3 ABOUT THIS THESIS

This research aims to provide an advanced control algorithm for the solar micro-inverter system. A deadbeat controller, called one-sampling-ahead-preview (OSAP) is proposed as the inverter controller. Fig. 1.6 shows the basic circuit of a single-phase grid-tied photovoltaic micro-inverter, which is analysed in this thesis. An advanced PV control system is proposed to improve the performance of existing solar systems. Both simulation and experiment results are provided to support the theoretical analysis.

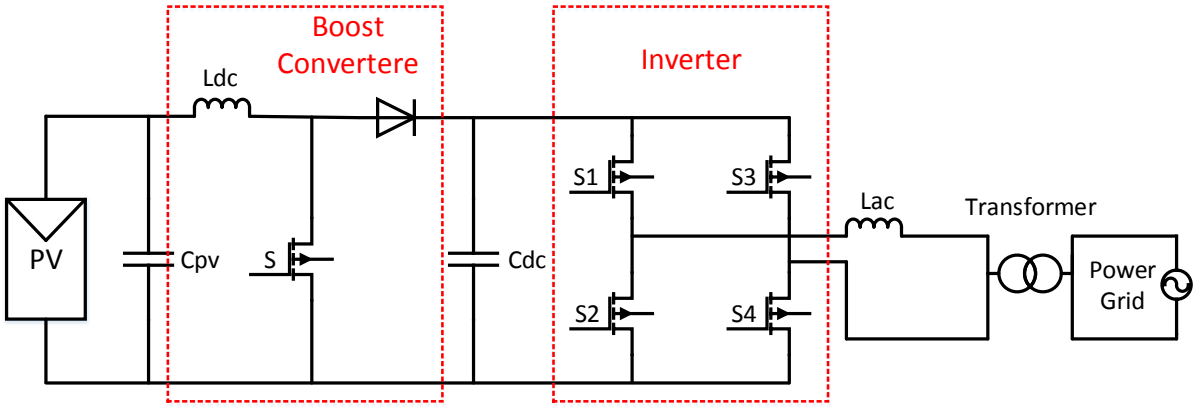

Figure 1.6: The reaearch circuit in this thesis

The structure of this thesis is shown as follows: Chapter 2 introduces the characteristics of solar cells and MPPT techniques to optimize the output power of solar panels. Chapter 3 focuses on the functionality of a full-bridge single-phase inverter. Two different states of this inverter are analysed respectively and deadbeat controllers are applied in each scenario. Afterwards, an improved deadbeat controller is proposed to overcome the drawbacks of the existing one. Simulation results are also given to support the analyses. Chapter 4 explains the experiment of this solar system. The experimental results are also shown to demonstrate the theory. Chapter 5 presents the conclusion of this research and the future work that could be done.

Chapter 2

SOLAR CELLS AND MPPT CONTROL

2.1 INTRODUCTION

Solar cells, as the energy provider, form a basic part of a PV system. Unlike a conventional DC source whose output can be kept constant during operation, both environmental changes and their own characteristics have a significant influence on the output power of solar cells. Thus, getting a full understanding of solar cells has great importance. A maximum power point (which is also called MPP) of a solar cell always exists and changes along with the environment. This MPP ensures a solar cell can generate its maximum power according to the current conditions. In order to maximize the PV system efficiency, this MPP should be kept during operation. A technique called maximum power point tracking (MPPT) is designed specifically for solar cells to track the MPP.

In this chapter, a solar cell is analysed and mathematically modelled. Based on this model, an improved model which is suitable for simulation is adopted. With this simulation model, the influences of environmental changes (i.e. the temperature and irradiation) can be analysed. Several MPPT techniques are investigated and compared. Based on these analyses, a more advanced MPPT technique is proposed to overcome the known disadvantages of the conventional MPPT algorithms. Simulation results are also attached to demonstrate the MPPT operation.

2.2 PHYSICS CHARACTERISTICS OF SOLAR CELLS

Brief studies performed by *Photon International* show that almost $47.5GW_p$ of PV modules had been manufactured in 2014 worldwide. Given the average price of electricity from solar industry is still higher than the conventional electrical sources, scientists are seeking more suitable materials and applying more advanced technologies in PV field. For now, several materials have already proven their reliability and acceptable price, such as silicon solar cells and thin film solar cells. Table 2.1 provides an overview of the contribution of power generation from PV panels

based on different materials in 2008 and 2014 respectively. All the PV modules have experienced a huge increase in power generation in the 6 years. Crystalline Si (Multi-Si, Mono-Si and Ribbon-Si) has dominated the whole market for at least 6 years (87% in 2008 and 90.7% in 2014) and is still being the most popular material for solar cells. Despite being the minority of the market, thin film modules, consisting of amorphous silicon (a-Si), CdTe and CIS types, share a significant growth from 2008 to 2014. Other types of PV cells are still waiting for further development [11], [12].

Table 2.1: Total MW/GW of production and proportion of different kinds of solar cells in 2008 and 2014

Technology	2008		2014	
	MW	%	GW	%
Multi-Si	3773	48	26.2	55.1
Mono-Si	3024	38	16.9	35.6
Ribbon-Si	118	1	0	0
a-Si	403	5	0.8	1.7
CdTe	506	7	1.9	4
Cu(InGa)Se2	79	1	1.7	3.6
Total Crystalline Si	6915	87	43.1	90.7
Total Thin Films	988	13	4.4	9.3
Total	7910	100	47.5	100
Data from *Photovoltaic Report* and *Photon International*				

A relatively low price of silicon solar cells is the main reason for their popularity. Besides, efficiency is another major critical factor that will affect the popularity of PV cells. Studies show that high light absorption capability is an essential requirement for solar cell materials. Laboratory tests have demonstrated that the conversion efficiency of CIS and CIGS solar cells can reach as high as 20 percent. A multi-junction Si solar cell can produce better than 30 percent conversion efficiency. Improvements have also been made in the thin film of group III-V compound semiconductor materials, such as GaAs, InP, CIS, CIGS and CdTe. However, these high-efficiency solar cells require high-tech manufacturing processes, which will increase the production cost. Thus, despite that the majority production on the market is still low-efficiency solar cells due to their cheap price, a foreseeable evolution in PV cells production technology is possible [11], [12].

2.2.1 Crystalline Silicon Solar Cell

Crystalline solar cells are the most widely used solar cells, being responsible for about 90% of PV production worldwide. Silicon can be arranged in different forms to obtain a photovoltaic cell depending on crystal structure [13]. More specifically, c-Si modules are divided into multi-

crystalline (multi-Si), single- or mono-crystalline (mono-Si) and ribbon silicon, depending on the type of Si wafer used. Their efficiency ranges from 13% to 22% under laboratory environment. Several features have guaranteed the mass production of crystalline solar cells: Firstly, the enormous development of microelectronics, which is also based on Si material, offers a great help to the Si cell technology. Secondly, the band gap of silicon is optimal for a solar cell. In addition, Si solar cells are very stable, even without encapsulation [11].

Solar cell modules must reach a price level of $\$0.5/W_p$ to $\$0.2/W_p$ to become competitive with conventional coal or nuclear power generation. Achieving a cheap price requires several new technologies to be applied in the innovation of solar cells in the future. These new technologies include novel technologies to break through efficiency barrier of 25%; wafer slicing technologies and equipment for ultra-thin wafers ($50\mu m$); low-cost contact-forming technologies; materials providing performance comparable to mono-crystalline cells and so on [14].

2.2.2 Thin film Solar Cell

Silicon material is the best choice for the fabrication of solar cells due to its minimum cost. However, other applications also require large amount of silicon material and this demand creates a global shortage of silicon supply, which consequently pushes the price for silicon solar cells higher. Scientists are trying to find alternative materials to replace silicon and some new technologies have emerged. Thin film solar cell is among them and it has little or no dependence on silicon. Generally, there are three common types of thin film solar cells: amorphous silicon (a-Si) cells, cadmium telluride (CdTe) cells and copper indium gallium di-selenide (CIGS) cells. Since these cells are based on materials that have strong sunlight absorption capabilities, thin film solar cells could be made very thin, which is usually 1-3 micrometers. This advantage ensures the electrons only travel short distance from the inside to the cell contacts and then to the external circuit to generate power. Thus the demand for high purification and crystallinity of the material has been reduced, which is the main factor for the high price of Si cells. Furthermore, thin film cells are made and simultaneously formed as a module instead of a wafer [12].

Even though researchers had already known thin film semiconductors could make good solar cells, several disadvantages still remain and prevent the mass production of thin film cells. One major concern for thin film cells is the low efficiency. Generally, the efficiency of thin film modules is 25-50% lower than Si cells. Besides, as mentioned before, the technology of Si is already mature enough that Si cells can definitely benefit from this advantage. But for the thin film technology, it has to start from the beginning. The known strength leaves the thin film cells a bright future but there are remaining challenges in thin film industry [11].

2.3 PV MODELS

2.3.1 Mathematical Model

Having an accurate model of PV cell is of great importance for the solar system when dealing with dynamic analysis of power conversion, the choice of optimal control methodology, accessing the most suitable MPPT technology, the evaluation of solar system efficiency and above all, developing simulation tools to analyse PV systems [13]. Generally, a solar cell is an electronic device capable of converting the radiated energy obtained from sunlight into electricity. More specifically, the electrical characteristics of PV cell can be modelled as a current source in parallel with a diode shown in Fig. 2.1. A series resistor R_s has been added to represent the total power losses due to the current circulation through different parts of the device and a shunt resistor R_{sh} is to model the effect of leakage current of the $p-n$ junction [13].

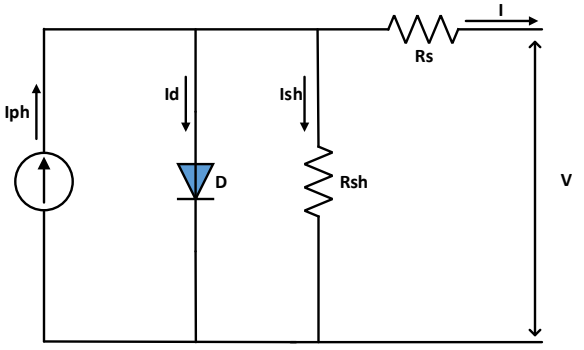

Figure 2.1: PV cell circuit model

Based on the circuit model of PV cells, the basic equation that analytically describes the $I-V$ characteristics of ideal solar cells can be obtained as follows [13]:

$$I = I_{ph} - I_s(e^{q(V+IR_s)/A_qkT} - 1) - \frac{V+IR_s}{R_{sh}} \tag{2.1}$$

where:

I	is the cell terminal current
V	is the cell terminal voltage
k	is the Boltzman constant $= 1.38 \times 10^{-}23J/K$
q	is the electronic charge $= 1.6 \times 10^{-}19C$
T	is the PV cell temperature
I_s	is the saturation current of diode
A_q	is the diode reality factor
I_{ph}	is the photo-generated current, linearly depending on solar irradiation
R_s	is the equivalent series resistor
R_{sh}	is the equivalent shunt resistor

2.3.2 Simulation Model

Since the mathematical model of a PV cell has already been obtained, the next step is to build the simulation model of solar cells in software. In this research, Matlab has been used to execute simulation studies of PV systems. In order to solve the nonlinear equations of PV cell output current I and output voltage V shown in Eqn. 2.1, the Newton-Raphson method has been adopted. If properly used, this iterative method homes in on a root effectively [15].

In Eqn. 2.1, there are five variables: I_{ph}, I_s, R_s, R_{sh} and A_q. Usually these variables are dependent on the temperature, the irradiation and PV cell itself . However, these variables are usually not provided by the PV cell manufacturers. Eqn. 2.1 is not a suitable model for implementation and a simplified solar cell model for simulation has to be developed. In [16], an engineering analytical model of solar cells have been developed with the assumption that: ① $(V + IR_s)/R_{sh}$ are ignored because the leakage current is usually far less than the photo-generated current; ② $I_{ph} = I_{sc}$ because usually equivalent series resistance R_s is far less than the diode resistance when turned on. With these parameters (I_{sc}—short-circuit current, V_{oc}—open-circuit voltage, I_m—MPP current and V_m—MPP voltage) obtained from the datasheet provided by the manufactures which are recorded under standard test conditions (i.e. PV cell temperature $T_{ref} =$ 25℃, PV cell irradiation $S_{ref} = 1000W/m^2$), we can approach the real values of $I'_{sc}, V'_{oc}, I'_m, V'_m$ under different temperature and irradiation as closely as possible with Equation set 2.2:

$$\begin{cases} \Delta T = T - T_{ref} \\ \Delta S = \frac{S}{S_{ref}} - 1 \\ I'_{sc} = I_{sc} \times \frac{S}{S_{ref}}(1 + a\Delta T) \\ V'_{oc} = V_{oc}(1 - c\Delta T)\ln(e + b\Delta S) \\ I'_m = I_m \times \frac{S}{S_{ref}}(1 + a\Delta T) \\ V'_m = V_m(1 - c\Delta T)\ln(e + b\Delta S) \end{cases} \tag{2.2}$$

Where the typical value of a, b, c is:

$$a = 0.0025/^{\circ}C, b = 0.5, c = 0.00288/^{\circ}C \tag{2.3}$$

According to [16], the simplified form of Eqn. 2.1 is:

$$I = I_{sc}[1 - C_1(e^{\frac{V}{C_2 V_{oc}}} - 1)] \tag{2.4}$$

Where:

$$\begin{cases} C_1 = (1 - \frac{I_m}{I_{sc}})e^{\frac{-V_m}{C_2 V_{oc}}} \\ C_2 = 11 \end{cases} \tag{2.5}$$

Calculating the values of I'_m, V'_m, I'_{sc} and V'_{oc} from Equation set 2.2 with the temperature and irradiation measured under current environment conditions, substituting theses parameters into Eqn. 2.4, an accurate solar cell model is built. Running simulation with this PV model, we can easily and accurately simulate the PV cells and record the output values for further studies.

2.3.3 Simulation Research

The simulation model being built in Matlab is shown as Fig. 2.2:

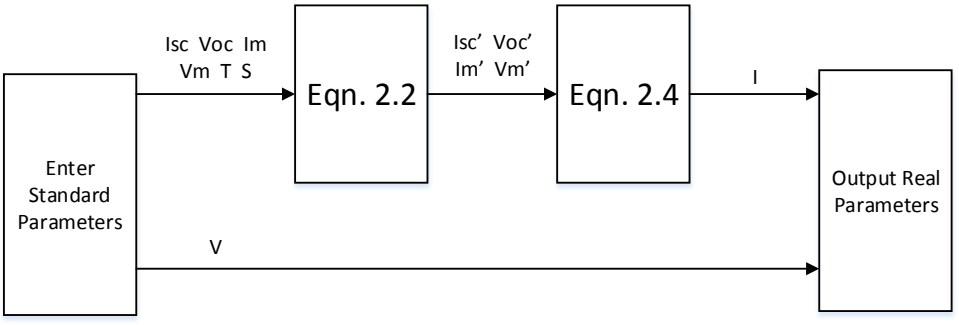

Figure 2.2: The simulation model of PV cells in Matlab

All the solar panel data applied in this research project about the solar panel is from the product of SOLAR POWER—the SP Series Solar Module Model SP205. The electrical characteristics are shown in Table 2.2. In this thesis, all the simulation and experiments of solar cells are based

on this solar module.

Table 2.2: Electrical characteristics of SP205

Model Number	SP205	Cell Type	Mono and Multi-Crystalline Si
Maximum Power	$205W$	No. of Cells	54
V_{mpp}	$25.80V$	I_{mpp}	$7.95A$
V_{oc}	$32.60V$	I_{sc}	$8.48A$
Fuse Rating	$15A$	Maximum System Voltage	$600V$ (UL)/ $1000V$ (IEC)
Temp. Coefficient of V_{oc}	-0.341%/℃	Temp. Coefficient of I_{sc}	0.120%/℃
Power Tolerance	±3%	Testing Irradiation S_{ref}	$1000W/m^2$
Testing Temperature T_{ref}	25℃		

For a given irradiation and ambient temperature, making the solar cell output voltage V as the only variable, a certain output solar cell current I will be computed according to the values of V. Assuming that V ranges from 0 to V_{oc} and calculating the value of I, then a complete $I-V$ curve and $P-V$ curve are plotted in Fig. 2.3 that reflect the unique solar cell output current-voltage and power-voltage relationship from short-circuit condition to open-circuit condition.

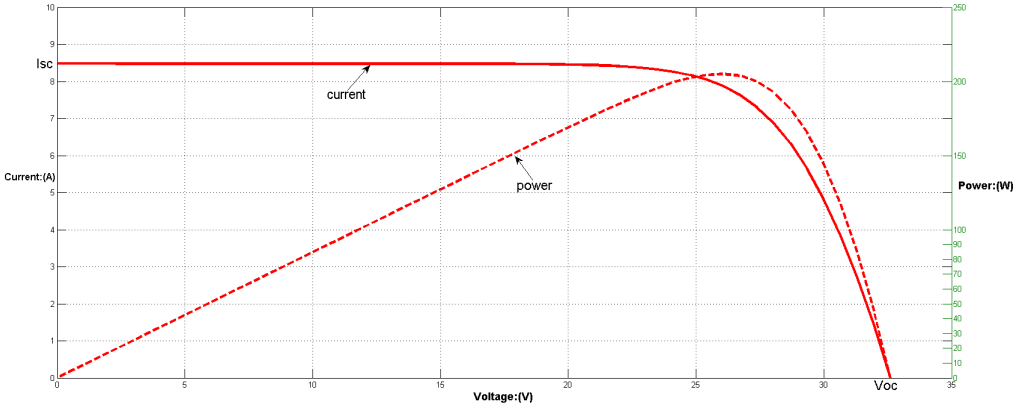

Figure 2.3: Simulation results of solar cell output current, voltage and power

When we simulate a PV system, environmental changes have to be taken into consideration because the changes in temperature and irradiation have important impacts on the output power of solar cells. In Fig. 2.4(a) and Fig. 2.4(b), the impacts of variable temperature and irradiation have been presented respectively. It shows lower the temperature and the higher the sunlight, the more power PV cells will generate.

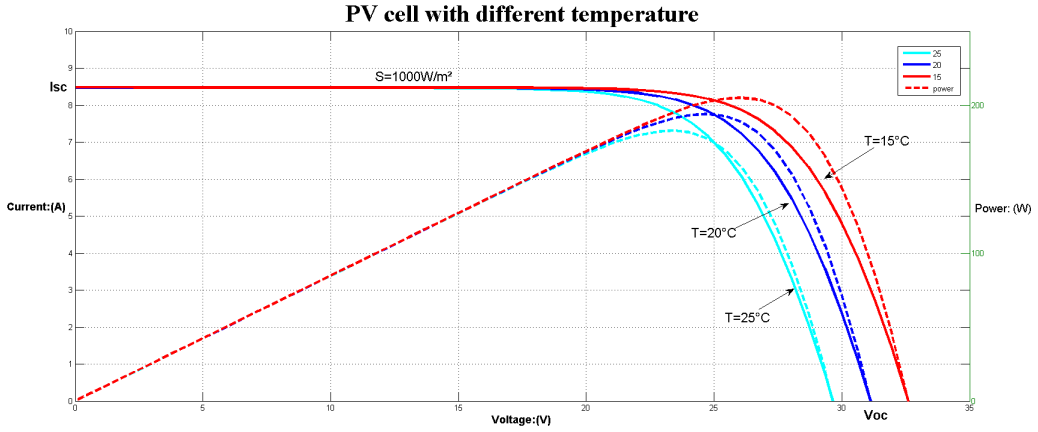

(a)

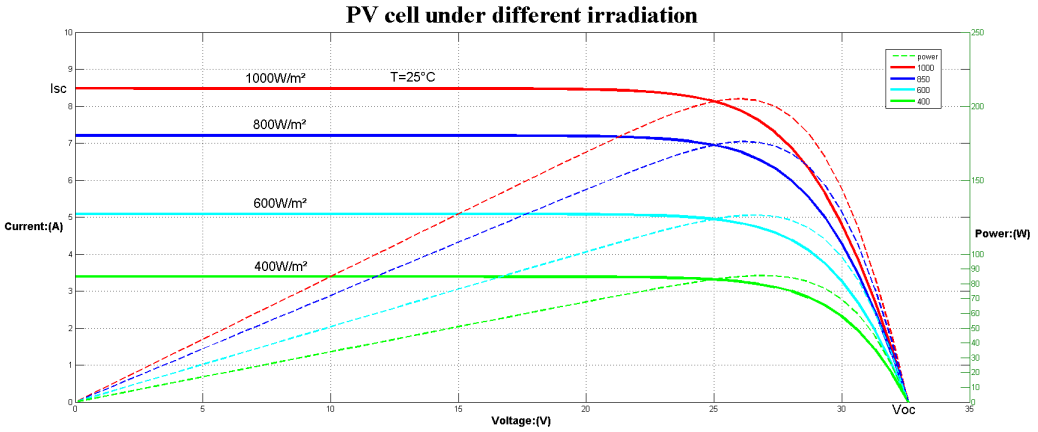

(b)

Figure 2.4: Simulation results of PV cells with environmental changes. (a) Constant irradiation and variable temperature (b) Constant temperature and variable irradiation

2.4 MAXIMUM POWER POINT TRACKING TECHNIQUES

2.4.1 Introduction

The relationship between the output current I_{pv} and voltage V_{pv} determines there is only one point on the curve that makes the solar cell generate maximum power, and this point is named the maximum power point (MPP). Without proper terminal conditions, the solar cell will not be kept at the MPP during operation, and according to the analyses and simulation results in Section 2.3, the environment conditions such as the solar temperature and sun irradiation will also have a significant influence on the MPP. Thus a series of control methodologies named the maximum power point tracking (MPPT) techniques are introduced to to keep the solar panels remaining at the MPP during operation.

Different MPPT methods can be categorized based on their performance. In [17], a category is proposed based on their dependency on solar cell models. This category includes offline methods, online methods and hybrid methods. Offline and online methods can also be referred to as the model-based and model-free methods respectively [17]. Fig. 2.5 illustrates the details of this category for MPPT.

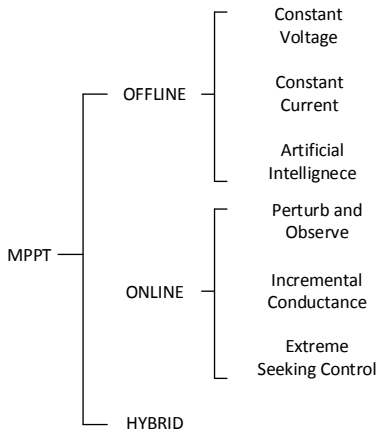

Figure 2.5: The category for MPPT

Offline methods generally depend on a known model of the solar cells and require one or more values to be measured periodically. These values could be the short-circuit current I_{sc}, open-circuit voltage V_{oc}, solar temperature T and irradiation S. By utilizing these measured values in the solar model, the controller can calculate the related MPP and force the system to track that point. By contrast, online methods usually record the instantaneous values of the solar cells to track the reference point. Since this kind of MPPT does not rely on the model of solar cells, they focus more attention on the response of PV cells for the perturbation introduced by the controller, and the next reference signal is based on this response. The hybrid methods are the combination of the offline and online methods, tracking the MPP into two steps: estimation and regulation [17].

In this section, three MPPT techniques—Constant Voltage MPPT which belongs to the offline methods, Perturb and Observe MPPT and Incremental Conductance MPPT which are among the online methods—are reviewed and analysed respectively. A comparison of complexity, dynamic response, steady-state error, robustness and efficiency of each technique is also proposed.

2.4.2 Constant Voltage MPPT

The simplest and fastest method to achieve MPP is Constant Voltage MPPT (or Constant Current MPPT) [18]. The theory of Constant Voltage MPPT is based on the assumption that

V_{mpp} is linearly dependent on V_{oc} (or I_{mpp} depends on I_{sc} in Constant Current MPPT) under variable environmental conditions. The fact is that the ideal MPP will always be very close to the assumed point regardless of the slightly changed environment during a period of operation. However, even though both Constant Voltage MPPT and Constant Current MPPT share the same theory, the voltage tracking technique is much more popular than the current tracking method for a simple reason: Based on the $I - V$ curve of a solar panel, usually there exists a significant difference between V_{mpp} and V_{oc} while I_{mpp} is very close to I_{sc}. In addition, measuring I_{sc} during operation is problematic, an additional switch is needed between solar panel and power converter to periodically short PV panel and get the short current value. This will definitely increase the complexity of PV circuit as well as the cost [19]. Thus constant voltage method is easily applied and more accurate than constant current method. The relationship between V_{mpp} and V_{oc} in Constant Voltage MPPT method is expressed as:

$$\frac{V_{mpp}}{V_o} = K \tag{2.6}$$

where K is a constant of proportionality and depends on the characteristics of PV panel and the current environmental conditions. K has to be computed before PV system operation. The normal value of K is usually chosen between 0.71 and 0.78 [19].

However, it has to be clearly stated that this sort of MPPT techniques are not a real MPPT method. V_{mpp} and I_{mpp} are chosen just based on an assumption, the accurate MPP is never reached because the MPP changes with the environment and the environment is never constant. Disturbance and the uncertain physical characteristics of PV panels will also contribute to the inaccuracy. But these methods can be applied when accurate MPP is not necessarily required. Actually, even though the power set by this algorithm is not exactly the maximum power, the output power of PV panels is not far away from the ideal value as long as shading problems do not occur [19]. And [20] points out K is no longer valid in the presence of practical shading of PV array.

2.4.3 Perturb and Observe MPPT

Perturb and Observe (P&O) and Hill Climbing algorithms are the most commonly used MPPT methods in practice. P&O and Hill Climbing are both based on the concept of perturbation—P&O introduces a perturbation into PV panel voltage while Hill Climbing conducts a perturbation in the duty cycle of the connected DC converter. The popularity of P&O and Hill Climbing is mostly due to the ease of implementation and relatively high accuracy.

Fig. 2.6 explains the operation process of P&O MPPT. Firstly, the original voltage is at point A with panel voltage V_1 and the corresponding output power P_1. Then the controller introduces a perturbation voltage $+\Delta V$ to V_1 and the panel is forced to work at V_2 at point B. Now P_2 is

calculated based on V_2 and is compared with P_1. Since $P_2 > P_1$, the direction of the previous perturbation is confirmed and it drives the controller continuing adding $+\Delta V$ to V_2 and PV panel will work at point C in the next time interval. This process repeats until it gets to point D, the next point after point D is point E but the comparison of the power shows $P_5 < P_4$, this result forces the voltage moving backwards, indicating in next time interval, a $-\Delta V$ instead of $+\Delta V$ will be added to V_5 and the operation point goes back to V_4 again. Fig. 2.7 is the flowchart of P&O MPPT algorithm.

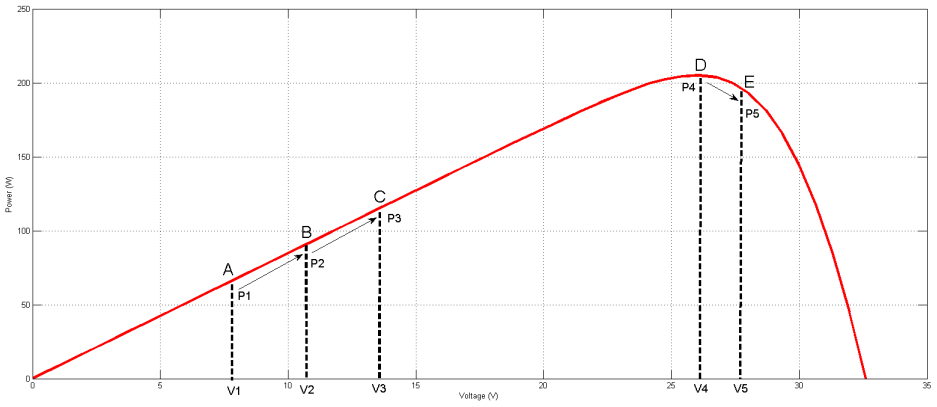

Figure 2.6: P&o MPPT operation progress

Despite the simplicity of implementation, P&O MPPT has some significant disadvantages. The whole process is executed periodically until it closely reaches the MPP. Then the system will oscillate around MPP since the exact MPP will be reached only with the appropriately chosen ΔV. This oscillation may introduce some power losses. In order to prevent or at least minimize the oscillation, reducing the perturbation step size is a good choice. However, a small step size slows down the tracking speed and it becomes worse when PV panels are under rapidly changing weather conditions [19]. Thus, as a trade off between the accuracy and speed, a two-stage algorithm is proposed in [21] that introduces a variable step-size MPPT. When in first stage where the operation point is relatively far away from the estimated MPP, a large ΔV is applied to reduce the tracking time. When it approaches the estimated point, a smaller step size is applied to achieve more accurate tracking results. Even though this variable step-size method can not totally remove the oscillation, it has been shown in [21] that it brings the operation point very close to the actual MPP with a few iterations, and is quite efficient during transient tracking phase, making itself suitable for fast changing environmental conditions.

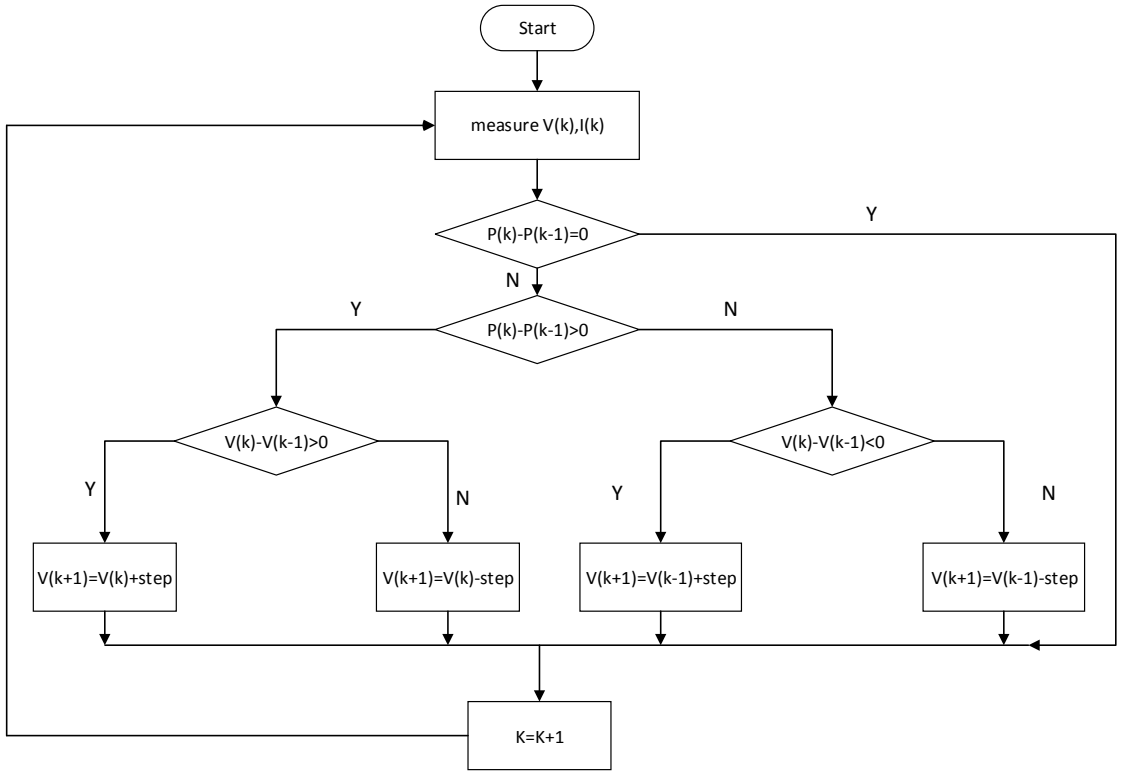

Figure 2.7: The flowchart of P&O MPPT

2.4.4 Incremental Conductance MPPT

Incremental Conductance (INC) MPPT algorithm relies on the fact that the slope of $P-V$ curve is zero at MPP (point B), positive on the left side (point A) and negative on the other side (point C) [19], it is shown in Fig. 2.8:

$$\begin{cases} \frac{dP}{dV} > 0, & \text{left of MPP} \\ \frac{dP}{dV} = 0, & \text{at MPP} \\ \frac{dP}{dV} < 0, & \text{right of MPP} \end{cases} \tag{2.7}$$

Since

$$\frac{dP}{dV} = \frac{d(IV)}{dV} = I + V\frac{dI}{dV} \cong I + V\frac{\Delta I}{\Delta V} \tag{2.8}$$

Eqn. 2.7 can be re-arranged as:

$$\begin{cases} \frac{\Delta I}{\Delta V} > -\frac{I}{V}, & \text{left of MPP} \\ \frac{\Delta I}{\Delta V} = -\frac{I}{V}, & \text{at MPP} \\ \frac{\Delta I}{\Delta V} < -\frac{I}{V}, & \text{right of MPP} \end{cases} \tag{2.9}$$

Hence, INC MPPT utilizes Eqn. 2.9 to search for the MPP. At the beginning of each sample

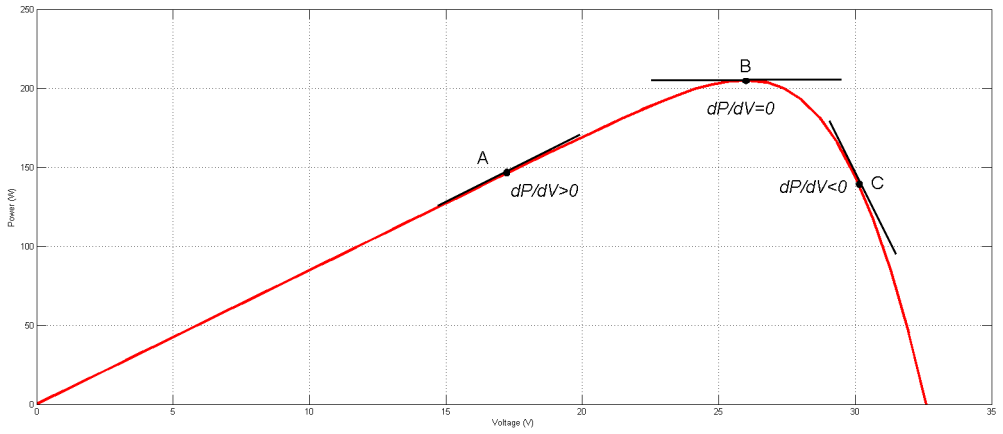

Figure 2.8: The slope of I-V curve

time, it compares the instantaneous conductance (i.e. I/V) to the incremental conductance (i.e. $\Delta I/\Delta V$) and get the direction of the perturbation voltage in the next time interval (i.e. $+V_{step}$ or $-V_{step}$). Once $\Delta I/\Delta V = -I/V$, the MP is reached and operation of MPPT will be held at that point unless a ΔI is noted, indicating a change in environment conditions as well as the MPP has occurred [19]. The flowchart Fig. 2.9 gives the details of INC MPPT algorithm.

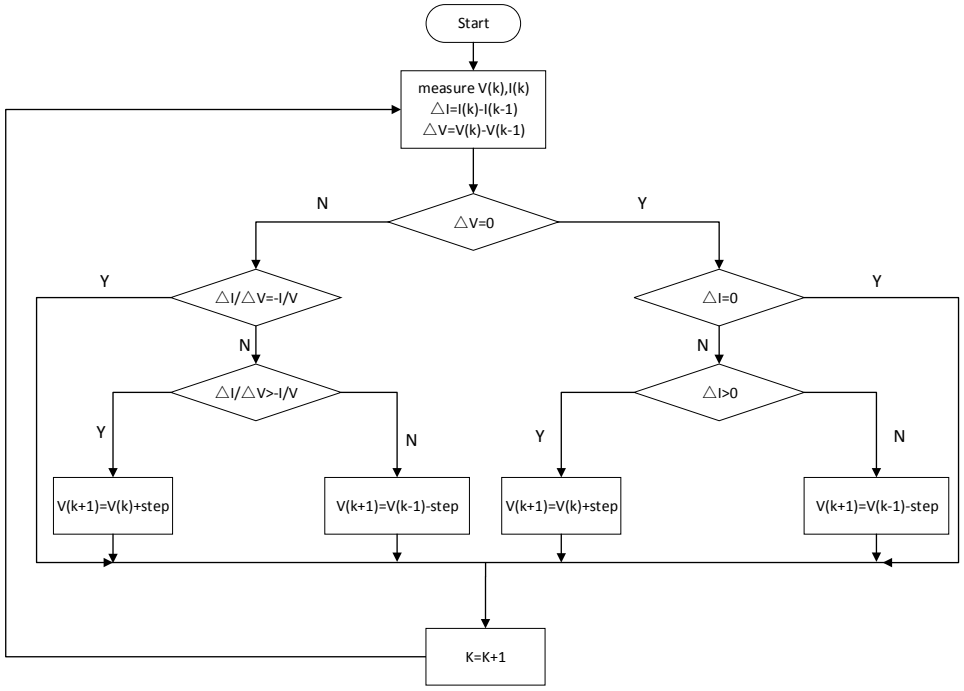

Figure 2.9: The flowchart of Incremental Conductance MPPT

Same as the P&O MPPT technique, the tracking speed and accuracy of INC MPPT algorithm also depends on the increment size (i.e. the perturbation voltage V_{step}). Oscillation can also be produced around MPP but can be suppressed with a more complex implementation [22]. Variable step-size method will also reduce the tracking time of INC MPPT. Generally, INC MPPT is superior to P&O method for several reasons: ① usually the tracking result of INC MPPT is much more accurate than the P&O MPPT; ② it can perform MPPT under rapidly varying irradiation conditions with higher accuracy [23]; ③ it ensures more stable performance when implemented on a microcontroller [24].

2.5 VARIABLE STEP-SIZE P&O MPPT TECHNOLOGY

As mentioned in Section 2.4, the performance of both P&O MPPT and INC MPPT is affected by the choice of step size. For a fixed step-size MPPT system, a larger step size contributes to faster dynamics while a smaller step size can bring low oscillation [25]. Tuning a suitable step size is a trade off between the tracking dynamics and tracking accuracy, which is usually a impossible task since the characteristics of solar cell continuously changing with the environment. An ideal solution is to force the MPPT controller to adapt the step size automatically based on the environmental conditions. Thus an improved MPPT technology called variable step-size MPPT is introduced to overcome this disadvantage.

Before discussing this improved method, a deeper study of the $P-V$ curve of solar cell is proposed here. Fig. 2.3 shows the typical $I-V$ and $P-V$ curves of solar cells. It is easy to notice that on the left side of the MPP (i.e. PV voltage is lower than V_{MPP}), the output power is almost linear to panel voltage and the slope of $P-V$ curve is nearly constant. But when it gets closer to the MPP, the slope drops down and finally reaches zero at the MPP. After it is over the MPP, the slope becomes negative and accumulates fast. Fig. 2.10 provides a clear image of the changes of the slope in the $P-V$ curve.

This unique characteristic of $P-V$ slope perfectly matches the need for the decision of perturbation step size: it becomes larger when the operation point is far away from the MPP while it decreases quickly when getting closer to the MPP, and most importantly, it stays zero at the MPP which indicates that oscillation is totally removed. Thus the slope of $P-V$ curve has been chosen for the decision of perturbation step size:

$$\Delta U = N \times |dP/dV| \tag{2.10}$$

The constant N is the scaling factor which is tuned based on the specific working condition of solar cell, ΔU is the step size of voltage perturbation.

By applying this variable step-size MPPT technique, several advantages can be achieved:

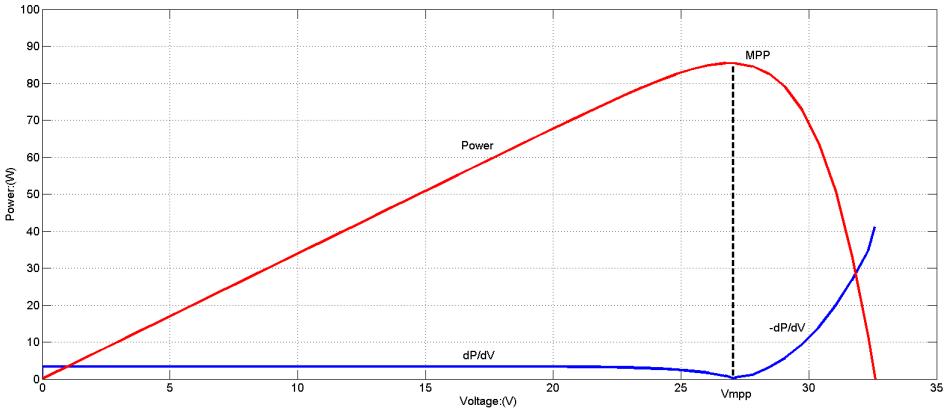

Figure 2.10: The slope of the P-V curve

1. When the current working point is far away from the MPP on the left side (which is the general condition at the beginning of operation), the step size is almost kept constant and tuning a relatively large N can get a short response time. When it is over MPP, the slope changes rapidly and a large step-size perturbation helps the system go back to MPP quickly.

2. When the MPP is exactly achieved, the slope of $P - V$ curve stays at zero, thus a zero step-size perturbation brings no oscillation to the system. Solar panel is kept at MPP until environment changes.

3. Even under slight environmental changes, the previously tuned N can work well for the changed conditions and no need to tune N again, which means the system is robust.

The flowchart of the improved variable step-size P&O MPPT has been shown in Fig. 2.11. Simulation results have also been provided.

Simulation results of a fixed step-size P&O MPPT and variable step-size P&O MPPT are shown in Fig. 2.12. Fig. 2.12(a) is the fixed step-size MPPT while Fig. 2.12(b) and Fig. 2.12(c) are for the variable step-size MPPT. Even though the fixed step-size MPPT has a faster response time with the $0.1V$ perturbation, significant oscillation is found when the system reaches the MPPT. By contrast, from the simulation results of variable step-size MPPT in Fig. 2.12(c), the perturbation voltage is $0.27V$ at $0.001s$ and it drops to $0.04V$ at $0.006s$. This shows the step size changes with the working point. The system is stable after $0.06s$ and the panel voltage is almost kept constant at $25.8V$, which is exactly the MPP of the solar panel. Oscillation has also been removed. Therefore, this improved variable step-size P&O MPPT can provide more accurate tracking result than the conventional techniques.

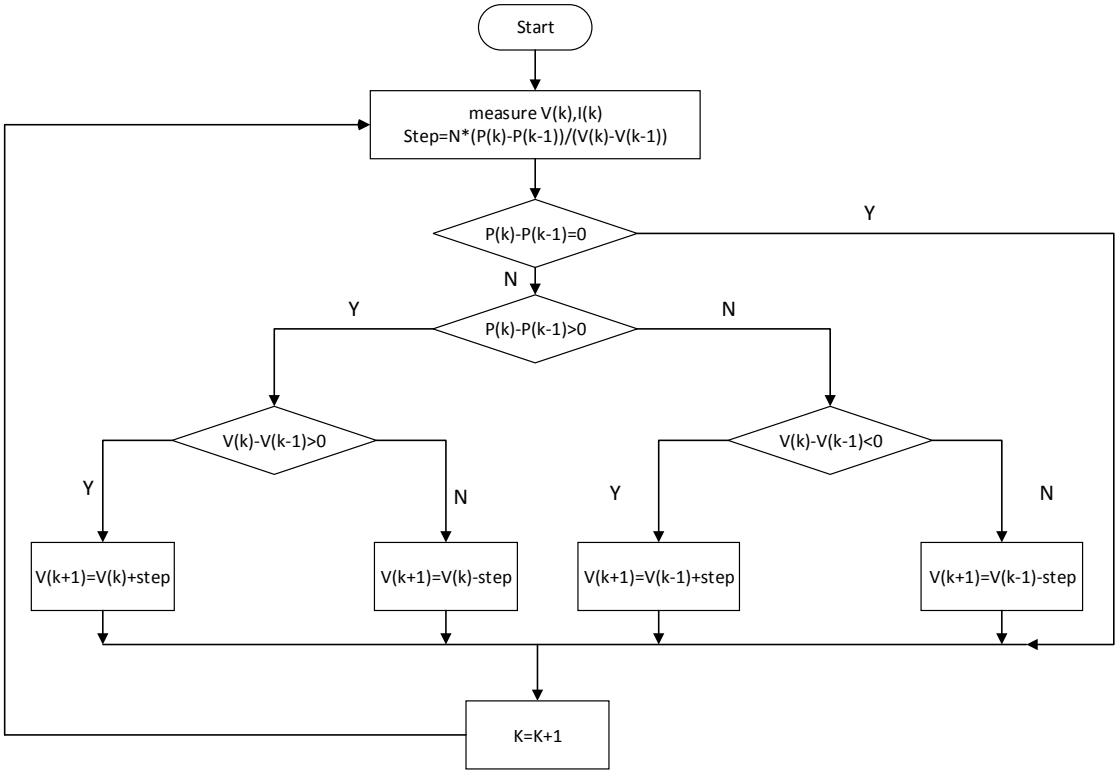

Figure 2.11: The flowchart of variable step-size P&O MPPT

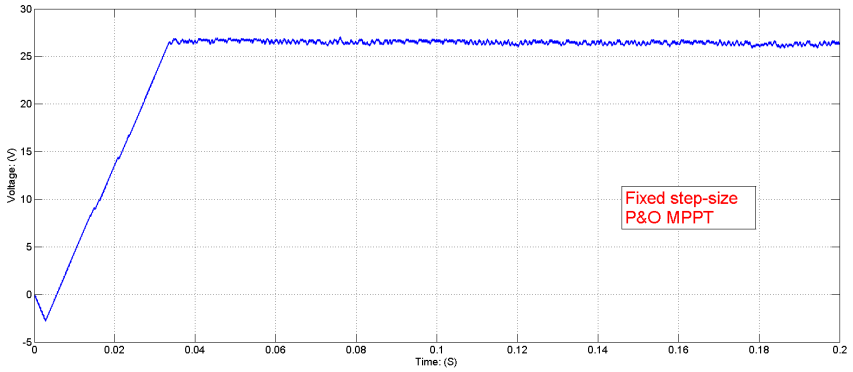

(a)

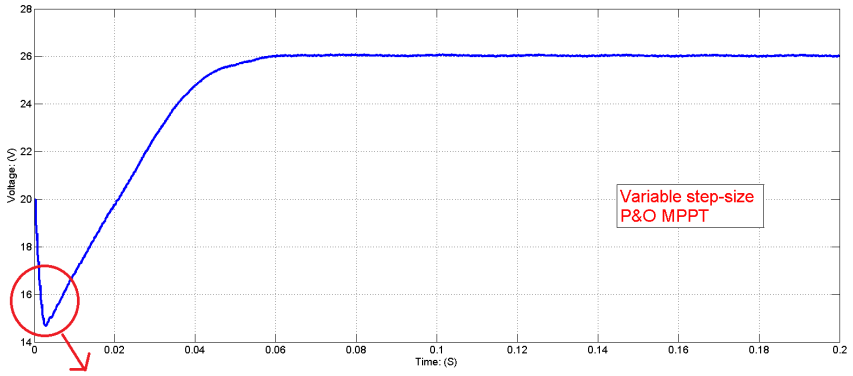

(b)

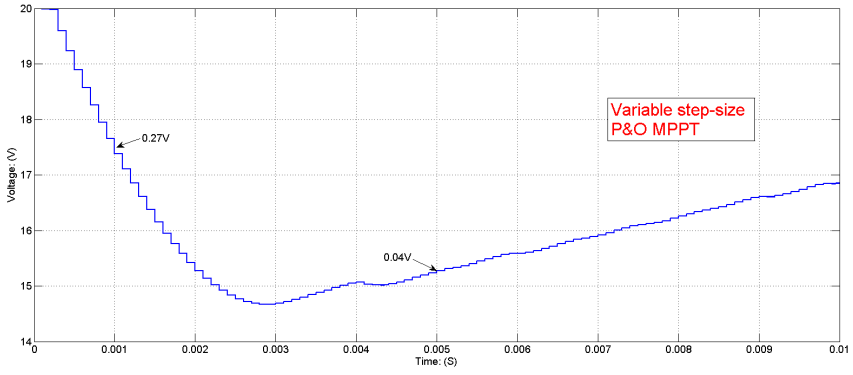

(c)

Figure 2.12: Simulation results of fixed step-size P&O MPPT in (a) and variable step-size P&O MPPT in (b) and (c). (a) Fixed step-size MPPT results (b) Variable step-size MPPT takes 0.06s to reach the MPP and brings no oscillation at around the MPP (c) Details show that the step size of voltage perturbation has changed in variable step-size MPPT

Chapter 3

THE INVERTER AND ITS CONTROL STRATEGY

3.1 INTRODUCTION

3.1.1 The Classification of Inverters

In this thesis, the DC-AC inverter is the interface between the solar panels and the power grid, transferring the power generated from PV side to the grid side. The utilization of power inverters requires application of control systems capable of providing high quality sinusoidal output current, minimizing disturbance, eliminating harmonics, synchronizing with the slightly changed grid frequency, regulating the active and reactive power and achieving immunity to grid perturbations [26]. Generally, as an important part of distributed generation system in a micro-grid, the functionality of DC-AC inverter is considered in both with On-Grid and Off-Grid conditions [27]. On-Grid means the power generated from DC source is fed back to the grid while Off-Grid condition is that inverters are required to feed power directly to local power consumers when there is no connection to the grid. Even though On-Grid is the general state that solar systems are expected to work in, sometimes inverters working under Off-Grid conditions are also very common, especially for residents living in remote areas where self-generated electricity can be the only solution.

In this chapter, two types of DC-AC inverter will be discussed: stand-alone inverters working in the Off-Grid situation and grid-tied inverters working in the On-Grid situation. In each section, a mathematical model of the inverter circuit is built. Different control strategies are proposed and analysed. A improved control algorithm is also presented to compensate the drawbacks of existing controllers discussed in previous sections. Simulation results are given to support the analysis.

3.1.2 Different Control Strategies For Inverters

Basically all control topologies can be classified as analogue controllers and digital controllers. Even though almost all control functions can be achieved with analogue (continuous-time) hardware and analogue control is relatively simple and robust, modern inverters still tend to adopt digital controllers instead of analogue controllers. The drawbacks of the analogue controllers are quite obvious: analogue controllers make it hard to provide accurate gains in the control loop because they highly depend on the electronic components, which have tolerances in reality; they can not provide interface for the operators so it is hard to tune a suitable gain in a control loop; it is hard to build an analogue controller in comparative logic and do MIMO (multiple input and multiple output). By contrasts, digital controllers have irreplaceable advantages: the flexibility of a digital controller means it can do really complicated control strategies and is easy to modify; they provide back-up functions and are quick to develop; they can do MIMO and have error detection functions; and maybe another important characteristic which is suitable especially for inverters is that digital controllers are capable of generating reference signals by themselves.

Several control strategies have been developed for inverters, they are listed below:

1. PI control
Proportional-integral (PI) controllers are widely used in modern control systems. Despite the advantages of PI controllers, which include feasibility and ease of implementation, this solution exhibits two well-known drawbacks for the inverter control: PI controller can not track a sinusoidal reference signal without steady-state error and poor disturbance rejection capability [28]. An alternative solution to overcome these drawbacks is using a second order generalized integrator (GI) [29].

2. Hysteresis control
Among the various PWM techniques available for inverters, the hysteresis band current control is adopted very often due to its simplicity of implementation. This method does not need any knowledge of load parameters so it can provide a fast response. The basic implementation of hysteresis current control is based on deriving the switching signals from the comparison of the current error with a fixed tolerance band. However, current control with a fixed hysteresis band has the disadvantage that the PWM frequency varies within a band during the fundamental period [30].

3. Deadbeat control
Deadbeat control is a typical example of linear control strategies implemented in discrete-time systems [31].The basic idea in a deadbeat control design is similar to the minimal prototype case: to achieve zero error at the sample points in a finite number of sampling periods for step references and step output disturbances. Deadbeat controllers are often used in inverter control due to their good dynamic properties. However, since the sampling period is the only design

parameter in a deadbeat control design, if the deadbeat response is desired, the designer must choose the sampling period carefully so that an extremely large control magnitude is not required in normal operation of the system. It is not physically possible to increase the magnitude of the control signal without bound. If the magnitude is increased sufficiently, the saturation phenomenon always take place [32]. So in the practical design, deadbeat controller usually comes with another controller in combination to form a usable controller. The controllers we apply in this research belong to the deadbeat control strategies.

4. Resonant control
The resonant control is basically based on the Internal Model Principle and has the capability of tracking a sinusoidal signal with zero steady-state error. It is an ideal controller for inverters. More details about resonant controllers will be discussed in Section 3.4.

3.2 STAND-ALONE INVERTER

3.2.1 Introduction

Formation of a microgrid system due to an islanding process is generally caused by a fault in power grid and its subsequent switching action, or a pre-planned switching event [33]. Under these Off-Grid circumstances, a microgrid is still supposed to keep providing stable power to the local customers connected to the power grid and fulfill the corresponding requirements for safety reasons. Inverters working under islanding conditions are usually called stand-alone inverters. In fact, as the only power provider in the network, the requirements for stand-alone inverters include providing protection for the connected equipment, ensuring stable voltage and current, minimizing the distortion and other essential requirements. The system performance in stand-alone mode is more sensitive to factors like control schemes and the types of loads [34]. In order to make sure all the components are working in a safe state, usually voltage control is adopted to stabilize the microgrid voltage. Current protection and harmonic distortion control are incorporated.

3.2.2 Stand-alone Inverter Model

The voltage-control stand-alone inverter topology shown in Fig. 3.1 consists of a stable DC Bus, full-bridge switches, a LC low-pass filter, and a resistive load R representing the power consumers. Unipolar SPWM (Sinusoidal Pulse Width Modulation) signals are generated by the controller and applied to drive the full-bridge switches. Mathematically, this DC-AC inverter can be modelled as a second-order system. In steady state, the output voltage V_o can be expressed

as:

$$V_o = V_{in} + V_L \tag{3.1}$$

Since:

$$V_L = L \cdot \frac{di_L}{dt} \tag{3.2}$$

$$= L\frac{d(\frac{V_o}{R} + C\frac{dV_o}{dt})}{dt} + V_o \tag{3.3}$$

Eqn. 3.1 can be expressed as:

$$LC \cdot \ddot{V_o} + \frac{L}{R} \cdot \dot{V_o} + V_o = V_{in} \tag{3.4}$$

Based on Eqn. 3.4, a state-space representation of this dynamic system can be obtained with a state vector $\begin{bmatrix} \dot{V_o} \\ \ddot{V_o} \end{bmatrix}$. The state-space equation of this inverter is obtained as follows [35]:

$$\begin{bmatrix} \dot{V_o} \\ \ddot{V_o} \end{bmatrix} = \begin{bmatrix} 0 & 1 \\ -\frac{1}{LC} & -\frac{1}{CR} \end{bmatrix} \begin{bmatrix} V_o \\ \dot{V_o} \end{bmatrix} + \begin{bmatrix} 0 \\ \frac{1}{LC} \end{bmatrix} V_{in} \tag{3.5}$$

where V_{in} is the switched DC input voltage on the AC side; L and C are the nominal values of the inductor and capacitor; R is the load resistance.

As mentioned before, Unipolar SPWM signals are applied to control this inverter. According to the control scheme, the switches in each leg of the full-bridge inverter are switched separately. Four combinations of switch on-states and the corresponding voltage levels are expected as:

1. S_1 and S_3 are ON: $V_{in} = 0$;
2. S_1 and S_4 are ON: $V_{in} = +V_{dc}$;
3. S_2 and S_3 are ON: $V_{in} = -V_{dc}$;
4. S_2 and S_4 are ON: $V_{in} = 0$;

The input voltage pulse is represented in Fig. 3.2 and this three-value switched voltage V_{in} can be expressed as:

$$V_{in} = \begin{cases} \pm V_{dc}, & \text{inside the period of } \Delta T \\ 0, & \text{outside the period of } \Delta T \end{cases} \tag{3.6}$$

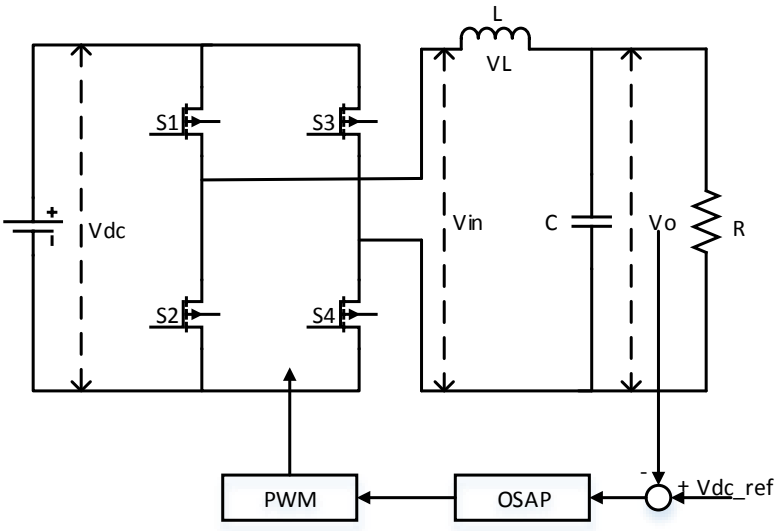

Figure 3.1: Stand-alone inverter circuit

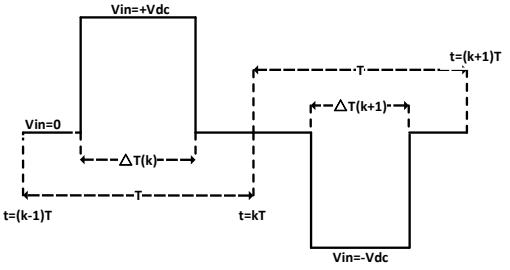

Figure 3.2: Input DC voltage pulse

3.2.3 OSAP Voltage Controller

Now we have obtained the mathematical expression of V_{in} and come back to Eqn. 3.5. It has been proposed in [36] that for a linear system $\dot{x} = Ax + Bu$, the forced state response equation can be written as:

$$x(t) = e^{At}x(0) + \int_0^t e^{A(t-\tau)}Bu(\tau)d\tau \tag{3.7}$$

Furthermore, its sampled-data equation can be expressed as [37]:

$$x(k+1) = e^{AT}x(k) + \int_0^T e^{A(T-\tau)}Bu(\tau)d\tau \tag{3.8}$$

Where T is the time step between sample k and sample $k+1$.

Let $\dot{X} = \begin{bmatrix} \dot{V}_o \\ \ddot{V}_o \end{bmatrix}$, $u = V_{in}$, $A = \begin{bmatrix} 0 & 1 \\ -\frac{1}{LC} & -\frac{1}{CR} \end{bmatrix}$, $B = \begin{bmatrix} 0 \\ \frac{1}{LC} \end{bmatrix}$ and $u = V_{in}$, the sampled-data form of Eqn. 3.5 at $t = kT$ with the assumption $T \ll 2\sqrt{LC}$ is [38]:

$$\begin{bmatrix} V_o(k+1) \\ \dot{V}_o(k+1) \end{bmatrix} = \begin{bmatrix} \varphi_{11} & \varphi_{12} \\ \varphi_{21} & \varphi_{22} \end{bmatrix} \begin{bmatrix} V_o(k) \\ \dot{V}_o(k) \end{bmatrix} \pm \begin{bmatrix} g_1 \\ g_2 \end{bmatrix} \Delta T(k) \tag{3.9}$$

Where:

$$\varphi_{11} = 1 - \frac{T^2}{2LC} \qquad \varphi_{21} = -\frac{T}{LC} + \frac{T^2}{2LC^2R}$$
$$\varphi_{12} = T - \frac{T^2}{2CR} \qquad \varphi_{22} = 1 - \frac{T}{CR} - \frac{T^2}{2LC} + \frac{T^2}{2C^2R^2}$$
$$g_1 = \frac{V_{dc}T}{2LC} \qquad g_2 = \frac{V_{dc}}{LC}(1 - \frac{T}{2CR})$$

In [37], an Autoregressive-moving-average model (ARMA) has been used to solve Eqn. 3.9, which yields:

$$V_o(k+1) = -p_1 V_o(k) - p_2 V_o(k-1) + m_1 \Delta T(k) + m_2 \Delta T(k-1) \tag{3.10}$$

Where:

$$p_1 = -(\varphi_{11} + \varphi_{22}) \qquad p_2 = \varphi_{11}\varphi_{22} - \varphi_{21}\varphi_{12}$$
$$m_1 = g_1 \qquad m_2 = g_2\varphi_{12} - g_1\varphi_{22}$$

Eqn. 3.10 clearly illustrates the relationship between the inverter output voltage V_o and the duty cycle $\frac{\Delta T}{T}$ of the SPWM. However, we cannot directly apply Eqn. 3.10 in the controller. $V_o(k+1)$ represents the inverter output voltage in the next interval, which requires an accurate preview value. This is impractical in the real life. This value should be replaced by a more practical one—the $V_{ref}(k)$. $V_{ref}(k)$ is defined as the voltage reference signal generated independently by the controller at $t = kT$. By replacing $V_o(k+1)$ with $V_{ref}(k)$ in Eqn. 3.10, we now have:

$$V_{ref}(k) = -p_1 V_o(k) - p_2 V_o(k-1) + m_1 \Delta T(k) + m_2 \Delta T(k-1) \tag{3.11}$$

Rearranging Eqn. 3.11, we can calculate the correct switch on time based on past and present variables:

$$\Delta T(k) = \frac{1}{m_1} V_{ref}(k) + \frac{p_1}{m_1} V_o(k) + \frac{p_2}{m_1} V_o(k-1) - \frac{m_2}{m_1} \Delta T(k-1) \tag{3.12}$$

This yields a deadbeat response $H(z) = z^{-1}$ and Eqn. 3.12 describes a one sampling ahead preview (OSAP) controller [35], [37]. This is the OSAP voltage controller that is applied to the stand-alone inverter in this thesis.

3.2.4 Simulation Research

The simulation model of this single-phase OSAP voltage-control inverter has been built in Matlab shown as Fig. 3.3. Table. 3.1 illustrates the details of each component in the circuit. This model utilises full knowledge of the inverter to digitally generate a switch control pattern that guarantees the desired inverter output voltage. This model is dependent on knowing all the system parameters—this is addressed in Section 3.4.

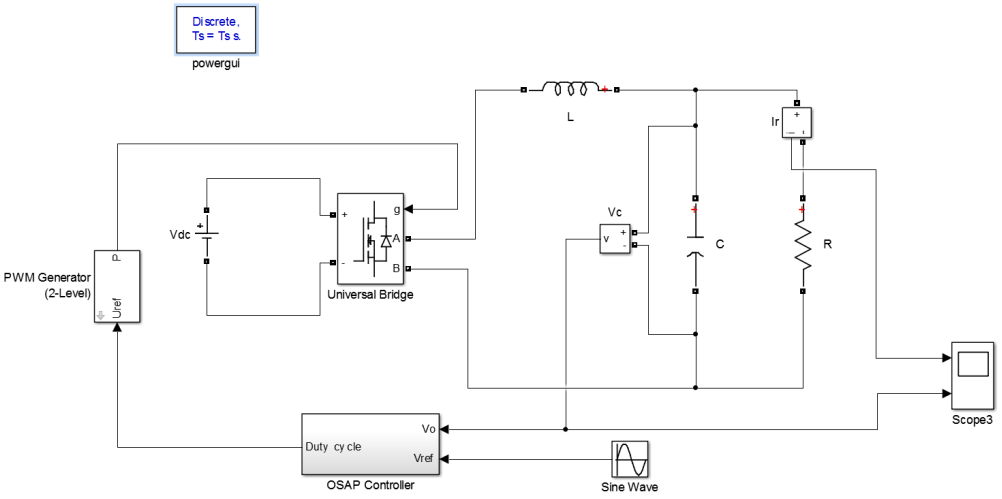

Figure 3.3: Simulation model of single-phase OSAP voltage-control inverter

Table 3.1: Parameters of single-phase OSAP voltage-control inverter

Output Voltage V_o	$21.2V$	Input Voltage V_{dc}	$60V$
Output Voltage Frequency	$50Hz$	Switching Frequency	$19200Hz$
Inductor L	$7mH$	Capacitor C	$24\mu F$
Resistor R	30Ω		

Details of the OSAP controller block is shown in Fig.3.4, and Fig. 3.5 shows the simulation results.

Fig. 3.5(a) shows the waveforms of the voltage reference signal V_{ref} and the inverter output voltage V_o and Fig. 3.5(b) is the error signal captured between V_{ref} and V_o. It is clear to see that there is a one-sample-time delay; this is caused by $V_o(k+1)$ being replaced by $V_{ref}(k)$ in Eqn. 3.12.

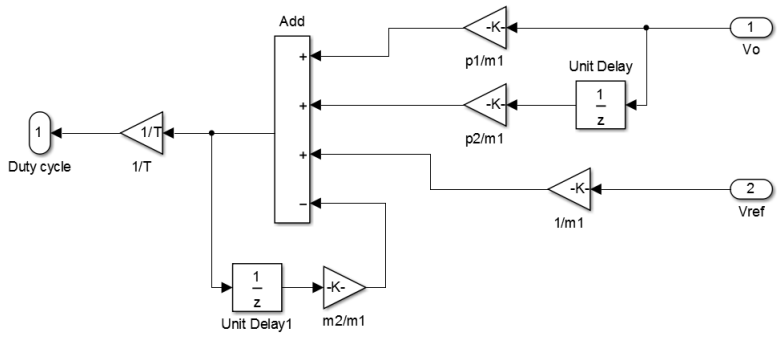

Figure 3.4: OSAP voltage controller

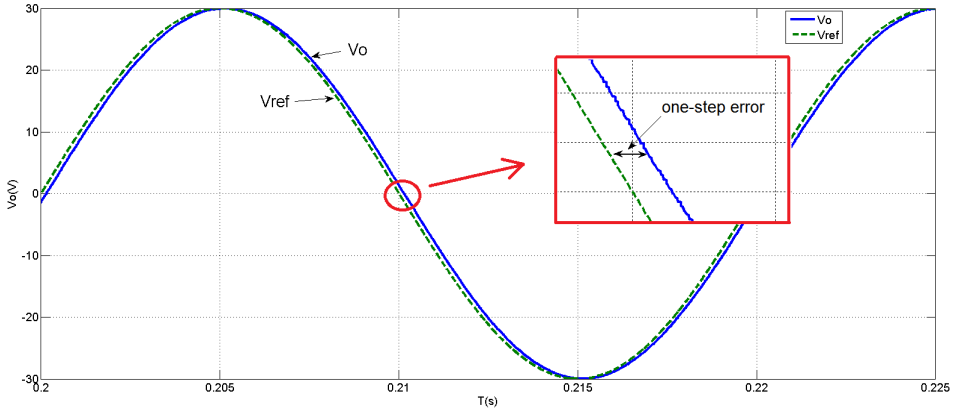

(a)

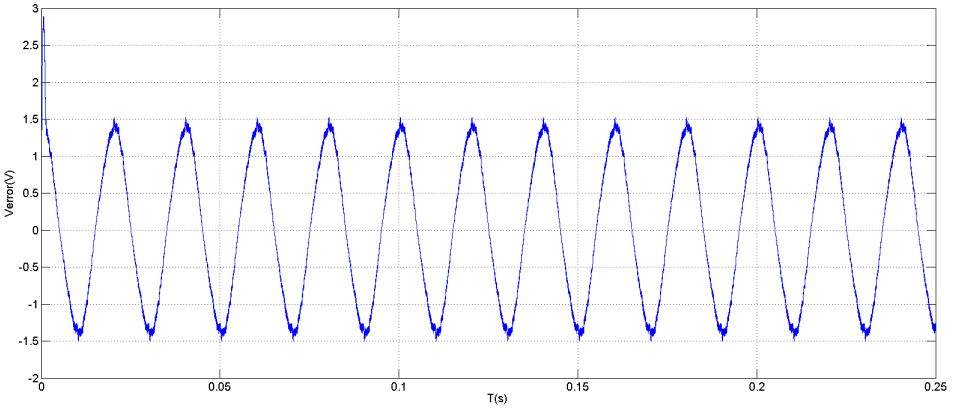

(b)

Figure 3.5: Simulation results of steady-state output voltage under OSAP voltage control. (a) Reference voltage V_{ref} with Output voltage V_o – one-step delay response. (b) steady-state error between V_o and V_{ref}.

3.3 GRID-TIED INVERTER

3.3.1 Introduction

Power systems are one of the most complex man-made dynamic systems, which require high-standard system capability to maintain stability and robustness. Similar to any dynamic system, the power grid also suffers from perturbations and experiences transitions from one operating state to another [39]. Even though significant contributions have been made to stabilize power systems since the day they were built, a lot of problems still remain. Generally, voltage stability, frequency stability and inter-area oscillations have become greater concerns than in the past [39]. For a grid-connected inverter which plays an important role in distributed generation systems, the ability to provide clean, stable, and safe power to the utility always has priority.

When DC power is converted into AC power, both voltage-control and current-control strategies are available. However, for grid-connected inverters the AC side voltage is determined by the grid; it is not easy for a small-scale micro-grid system to adjust the utility voltage. Thus Current controllers are usually chosen. In addition, current-control loops can run much faster than voltage-control loops, this advantage guarantees a fast response to short-circuit problems and helps improve the security of the power system.

3.3.2 Grid-tied Inverter Model

The topology of this grid-tied OSAP current-control inverter is shown in Fig. 3.6. As mentioned before, grid-tied inverters are required to feed "clean" current to the grid, where "clean" means ensuring low-level THD (Total Harmonic Distortion), synchronising current with the grid voltage and achieving unity power factor. These objectives are achieved by applying an OSAP current controller, which is similar to the OSAP voltage controller in Section 3.2.

In this thesis, an inductor is applied as the filter for this grid-tied inverter, and a resistor on the AC side is representing the resistance in power transmission lines. However, modern grid-tied inverters often have a more complex AC side filter, which is a LCL filter. This simple configuration is maintained in this thesis due to its simplicity and reasonable effectiveness. The model can be easily extended to more complex filter configuration if required.

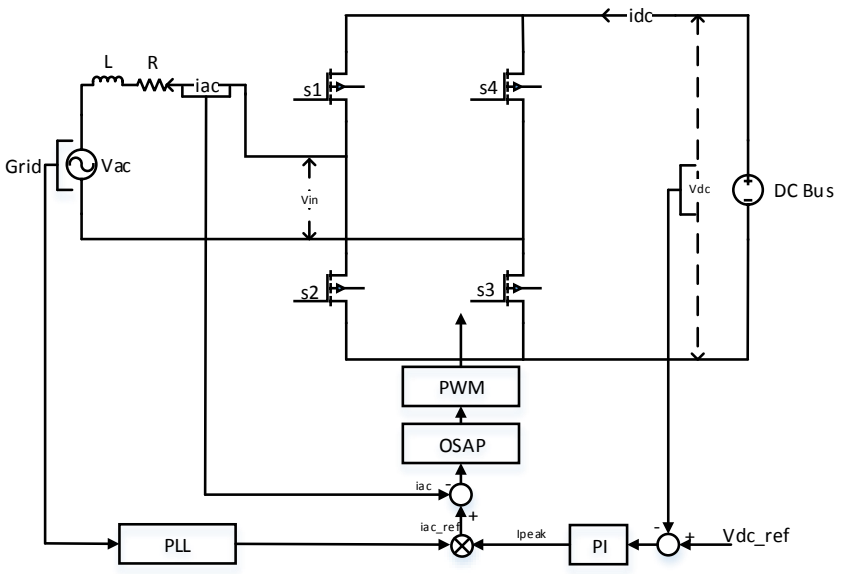

Figure 3.6: Grid-connected inverter with OSAP controller

Firstly, in the steady state, the equation of output current i_{ac} can be obtained as follows:

$$L \cdot \frac{di_{ac}}{dt} = V_{ac} - V_{in} - R \cdot i_{ac} \tag{3.13}$$

Or in the usual state space form:

$$\dot{i_{ac}} = \frac{-R}{L} \cdot i_{ac} + \frac{1}{L}(V_{ac} - V_{in}) \tag{3.14}$$

Different from the OSAP voltage controller, here Bipolar SPWM signals are applied to control the full-bridge switches. This is not a pre-requisite for an OSAP current controller, it is just chosen to be different from the voltage controller for the sake of completeness. The input pulse is shown in Fig. 3.7 and the switched V_{in} can be expressed as:

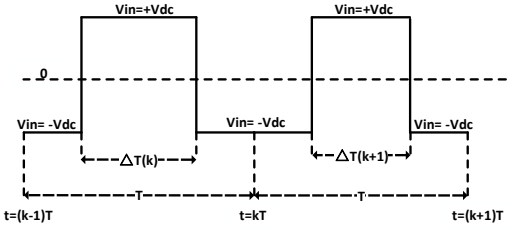

Figure 3.7: The input pulse of V_{in}

$$V_{in} = \begin{cases} +E, & \text{inside the period of } \Delta T \\ -E, & \text{outside the period of } \Delta T \end{cases} \tag{3.15}$$

More clearly:

$$V_{in} = (2 \cdot \frac{\Delta T}{T} - 1) \times V_{dc} \tag{3.16}$$

3.3.3 OSAP Current Controller

Since $\dot{x} = A \cdot x + B \cdot u$ can be rearranged as $x(k+1) = e^{AT}x(k) + \int_0^T e^{A(T-\tau)}Bu(\tau)d\tau$, the sampled-data form of Eqn. 3.14 at $t = kT$ is:

$$i_{ac}(k+1) = (1 - \frac{R}{L}T) \cdot i_{ac}(k) + \frac{T}{L} \cdot V_{ac}(k) - \frac{2\Delta T(k) - T}{L} \cdot V_{dc}(k) \tag{3.17}$$

The duty cycle of the SPWM can be obtained as:

$$\frac{2\Delta T(k) - T}{T} = \frac{1}{V_{dc}(k)} \left[V_{ac}(k) + \frac{L - RT}{T} \cdot i_{ac}(k) - \frac{L}{T} \cdot i_{ac}(k+1) \right] \tag{3.18}$$

Again, $i_{ac}(k+1)$ requires the AC current value at next sampling interval $(k+1)$ and this unknown value will be replaced by the AC reference current signal $i_{ref}(k)$, which results in a one-step response error:

$$\frac{2\Delta T(k)}{T} = \frac{1}{V_{dc}(k)} \left[V_{ac}(k) + \frac{L - RT}{T} \cdot i_{ac}(k) - \frac{L}{T} \cdot i_{ref}(k) \right] + 1 \tag{3.19}$$

Now the OSAP current controller has been presented, and the AC current reference signal i_{ac_ref} is needed. In some controllers, reference signals are given directly by the system operators, and an ideal current signal can also be provided for this controller. However, given that this output current is required to synchronize with the grid voltage and other factors have to be taken into consideration (e.g. power factor and reactive power compensation), it is not easy to get this ideal reference signal independently from the controller.

Generally, the voltage source connected to an inverter is a constant voltage source. But in this case, solar panels are the power source and their output voltage and current vary with the environment, which means these panels are a dynamically variable power source. Thus stabilization of DC Bus voltage is essential. In Chapter 2, the MPPT control strategy has been implemented and output voltage regulation has not been considered. In order to ensure a constant input DC voltage, DC voltage regulation is conducted by this inverter controller. A dual-loop control strategy has been applied in the controller. The structure of this dual-loop controller is shown in Fig. 3.8. It contains an external Proportional-Integral (PI) control loop

for the input DC voltage regulation, which is stabilized by the inner OSAP current control loop for the output AC current [40]. This is a reasonably common control strategy for this type of inverters.

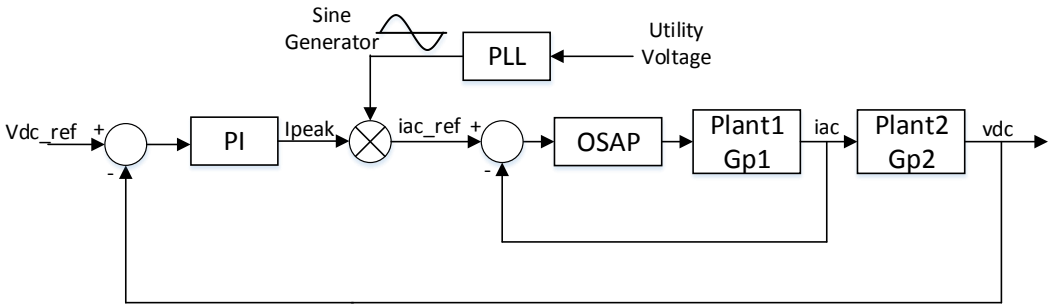

Figure 3.8: Dual-loop controller for grid-tied inverter

In this dual-loop controller, the current demand is generated from the power demand, and the power demand comes from the microgrid supervisory—the maximum power point of the solar panels, which is the system's capability of power generation [41]. In the external loop, DC bus voltage is forced to track a reference value V_{dc_ref}, which is set in advance as the desired DC Bus voltage. Then the error signal is fed into the PI controller and generates I_{peak}. Here I_{peak} is used as the amplitude of the reference signal for the inner current control loop. After multiplying by the normalized sine-wave coming from the utility tracking module, we get i_{ac_ref} as the current reference signal , which is in phase with the grid voltage and sets the output power. The OSAP current controller works with this reference signal to regulate the output current. This is the whole process of the dual-loop control strategy operation.

An issue for this dual-loop controller is tracking the utility voltage. Fig. 3.9 illustrates the details of the grid voltage tracking methodology. Except in some special situations where reactive power compensation is expected, reactive power must be minimized to maximize the amount of active power transferred across a congested transmission interface [42]. Here the reactive power Q is set as 0. In order to achieve unity power factor, a phase-locked loop (PLL) module is used to track the phase angle α of the grid voltage. With the combination of θ and α, a normalized $50Hz$ sine waveform can be generated. Multiplying this sine wave with the magnitude I_{peak} yields the current reference signal i_{ac_ref}.

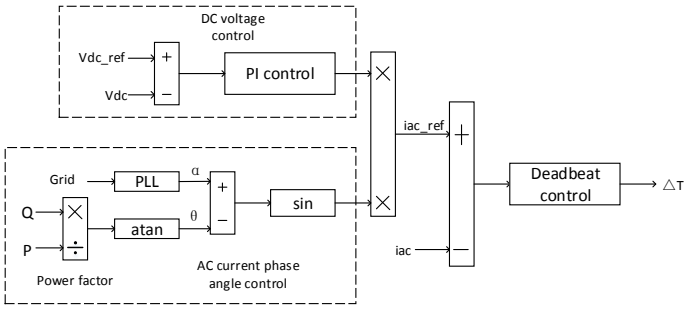

Figure 3.9: Grid-connected inverter control scheme

3.3.4 Simulation Research

A single-phase OSAP current-control rectifier has been modelled in Matlab, shown in Fig. 3.10. This rectifier shares the topology and control strategy with the grid-tied inverter shown in Fig. 3.6, where the DC Bus line has been replaced with a resistive load. Actually, the distinction between an inverter and a rectifier is artificial: a rectifier has much the same function as an inverter, in spite of the direction of energy flow [43]. The reason a rectifier is modelled instead of an inverter is that many rectifiers have a load whose output voltage depends on the load current, i.e. a resistor. This requires a control strategy to order a rectifier power that maintains the desired load power. A resistive load rectifier has been implemented rather than a constant voltage source so that there is a need for this sort of control. By contrast, modelling a dynamically variable DC source is relatively complicated. Table 3.2 gives the value of each component in this circuit.

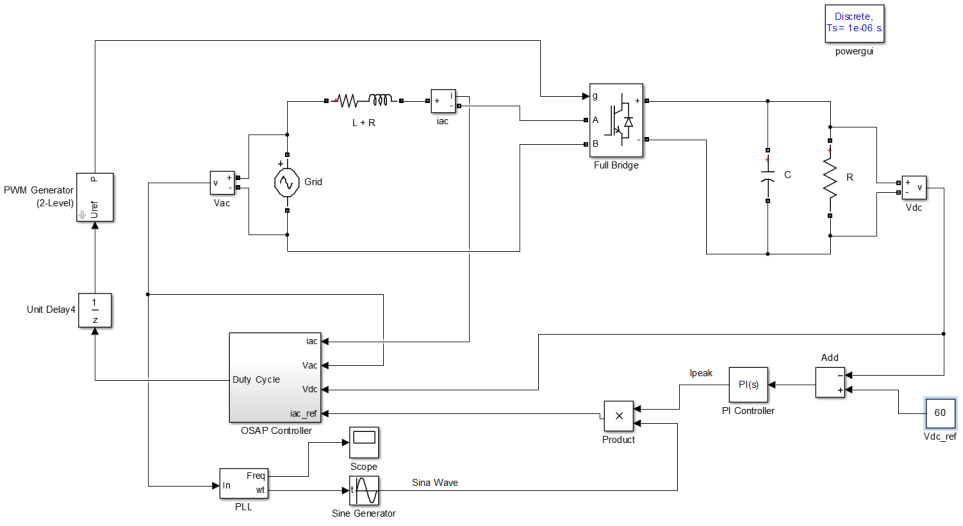

Figure 3.10: Simulation model of single-phase OSAP current-control rectifier

Table 3.2: Parameters of single-phase OSAP current-control rectifier

Grid Voltage V_{ac}	$21.2V$	DC Reference Voltage V_{dc}	$60V$
Grid Voltage Frequency	$50Hz$	Switching Frequency	$10000Hz$
Inductor L	$7mH$	Capacitor C	$0.3mF$
AC side Resistor R	0.3Ω	DC side Resistor R_{dc}	30Ω

Simulation results of a rectifier under OSAP current control are provided in Fig. 3.11. From Fig. 3.11(a), it is clear that there exists a one-step error between the current reference signal i_{ac_ref} and the output current i_{ac}. In Fig. 3.11(b), the DC side voltage V_{dc} is around $60V$ at steady state, which means the DC voltage regulation has been achieved. Fig. 3.11(c) also shows that the output current i_{ac} is in phase with the grid voltage V_{ac}. In a DC-AC inverter, the phase angle will be 180° instead of 0° in this AC-DC rectifier.

One problem must be stated here about this simulation model is the capacitor on the DC side. Actually this OSAP current control strategy is derived from the model shown in Fig. 3.6, where no DC capacitor is found and the DC Bus is a constant input. However it is common to find a capacitor on the DC side in a real inverter design. The reason a DC capacitor is needed is that in all inverter applications, the DC Bus faces high frequency ripple current due to the high frequency PWM switching and probably the current ripple introduced by the unstable DC source, thus a DC Bus capacitor is applied to reduce this ripple [44]. In this model, this DC capacitor and the AC inductor forms a "filter" by the connection of the full-bridge switches and noise at the resonant frequency of this "LC system" could exist. In this case, DC side voltage is not held constant and some voltage ripples are found in 3.11(b).

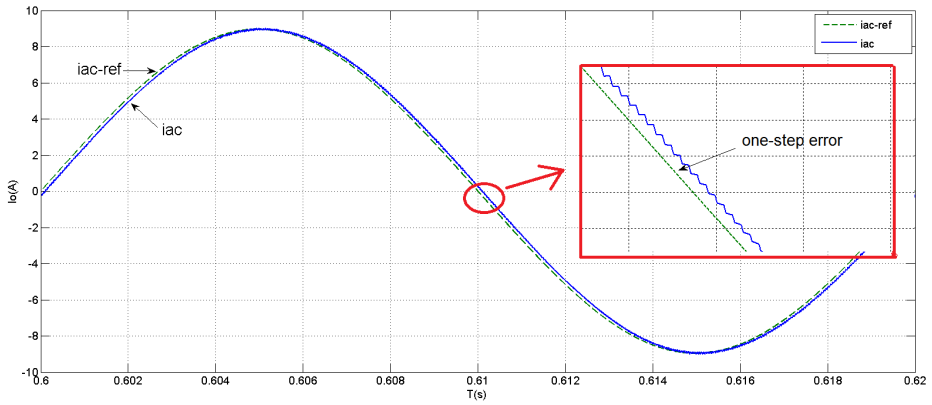

(a)

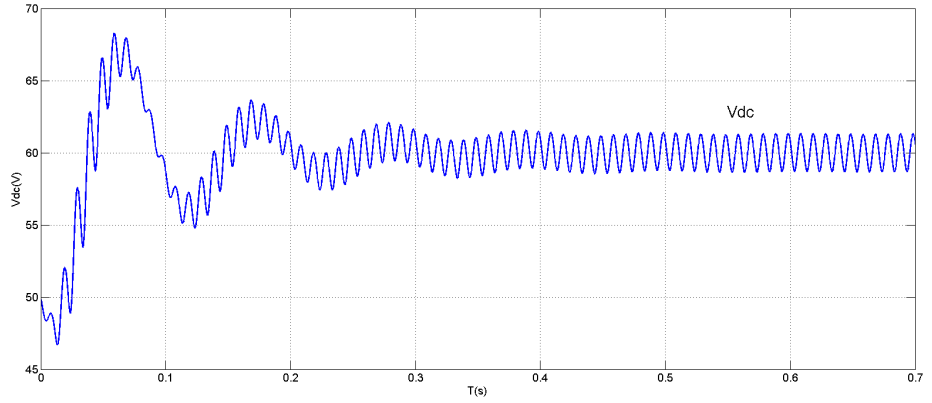

(b)

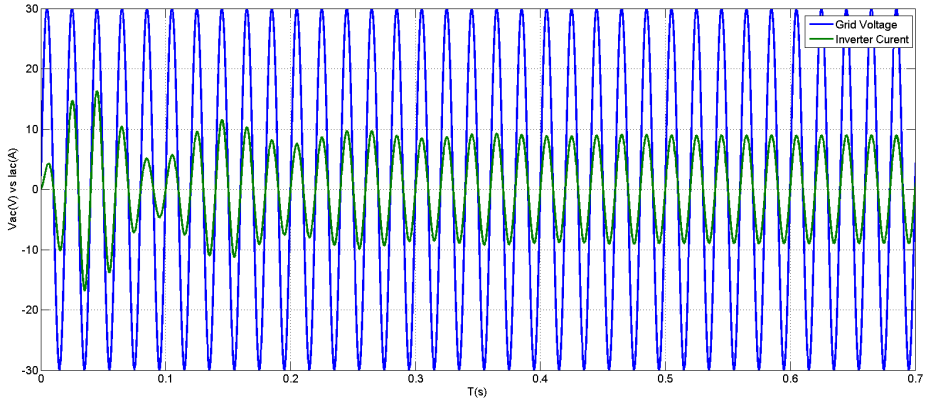

(c)

Figure 3.11: Simulation results of a single-phase rectifier with OSAP current controller. (a) One-step error of I_{ac}. (b) DC Bus voltage V_{dc}. (c) Grid voltage V_{ac} vs output current I_{ac}.

3.4 IMPROVED OSAP CONTROLLER

3.4.1 Errors Introduced By Component Tolerance

Even though OSAP controllers are easy to implement and have good dynamics, there are several disadvantages. Based on the analyses of the OSAP controller in Section 3.2 and Section 3.3, a future value is substituted with a present order value, yielding a one-step error between the reference signal and output signal. In addition, OSAP controllers rely on the model having accurate L, C and R values to get precise control gains. The tolerance of practical components as well as the uncertain electrical characteristics of power grid will bring uncertainties to the controller. These factors definitely cause tracking errors [37]. Fig. 3.12 illustrates the simulation results of an OSAP voltage-control inverter under practical conditions. This inverter model has exactly the same topology and components as the stand-alone inverter in Section 3.2, but this time this stand-alone inverter is treated as a practical inverter, which means the value of the L and C has a 10% tolerance (in this simulation, both L and C are assigned values 10% less than their normal values). The peak value of the output voltage is about $22V$, which is far from the reference voltage peak value $30V$. In order to achieve zero-error tracking, a Proportional-Resonant (PR) controller based on the Internal Model Principle is introduced in the next section to overcome uncertainties and improve tracking results.

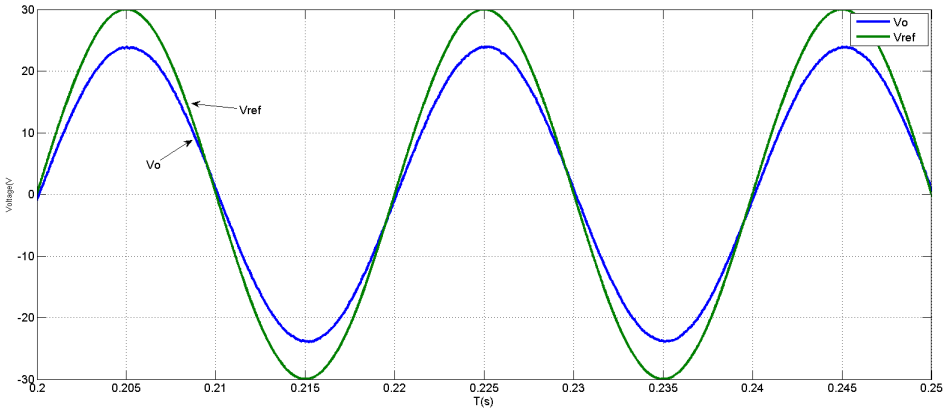

Figure 3.12: Simulation results of OSAP voltage-control inverter with uncertainties in component values

3.4.2 The Internal Model Principle

Proportional-Integral (PI) feedback control is widely used to eliminate steady-state errors and achieve zero-error tracking for linear time-invariant systems. However, the steady-state errors in periodic systems are dynamic and also periodic, the known drawbacks of PI controller are the

difficulty in removing the dynamic periodic errors and the limitations in bandwidth, which means eliminating low-order harmonics is impossible [45], [46], [47]. A controller called Proportional-Resonant (PR) control was introduced and has attracted attention due to its ability to overcome the known drawbacks of PI controllers.

Based on the Internal Model Principle, which states *"accurate control can be achieved only if the control system encapsulates, either implicitly or explicitly, some representation of the process to be controlled"*, a new control philosophy—Internal Model Control (IMC)—was championed by Francis and Woham in 1976 [48]. This control theory states that if the controller scheme has been developed based on an exact model of the process, then perfect control is theoretically achieved. A simple example of IMC is shown in Fig. 3.13 [49]:

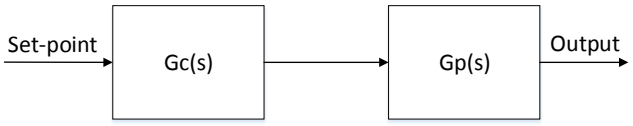

Figure 3.13: Internal Model control strategy

In this scheme, the controller $G_c(s)$ is applied to control the plant $G_p(s)$. Suppose the model of this plant has been built as $\widetilde{G_p(s)}$, which means mathematically $\widetilde{G_p(s)} = G_p(s)$. By setting $G_c(s)$ to be the inverse of the plant model, we have:

$$G_c(s) = \widetilde{G_p(s)}^{-1} \tag{3.20}$$

Obviously, the plant output would always be equal to the set point and zero-error tracking would be achieved, as long as the plant is perfectly known and there are no extended disturbances.

3.4.3 Resonant Controller

The model in Section 3.4.2 briefly illustrates the idea of internal model principle. [50] states that tracking a periodic signal in a linear plant is guaranteed if the controller contains the signal model to be controlled. Now we are back to the OSAP controller. Since the reference signals and the output signals dealt with in these inverters are all sinusoidal waveforms, the one-step error generated by the OSAP controller can also be represented by a sine-wave. In order to eliminate this error, if we embed the model of this sinusoidal error into the controller, zero-error tracking can be achieved. This controller is called a resonant controller.

The ideal PR controller is defined in Eqn. 3.21. A PR controller has exactly the same mathematical formulation in the s-domain as the standard sinusoidal waveform and this indicates the

appropriate IMC has been applied in the PR controller.

$$G_{PR}(s) = K_p + K_r \frac{s}{s^2 + \omega^2} \tag{3.21}$$

where K_p is the proportional gain, K_r is the resonant gain and ω is the resonant frequency.

Fig. 3.14 shows the Bode-plots of the PR controller, where the resonant frequency ω is chosen as $2\pi \cdot 50Hz$, $K_p = 1$ and K_r is set as 1. It can be seen that the PR controller achieves very high gain in a narrow frequency band centred around the resonant frequency (which is chosen as the grid frequency $50Hz$) and provides high attenuation for other frequencies. This unique characteristic guarantees that with the right choice of K_p and K_r, only those signals centred at the resonant frequency will be preserved. Thus, a resonant controller is the ideal choice for this grid-connected inverter dealing with errors at fundamental frequency.

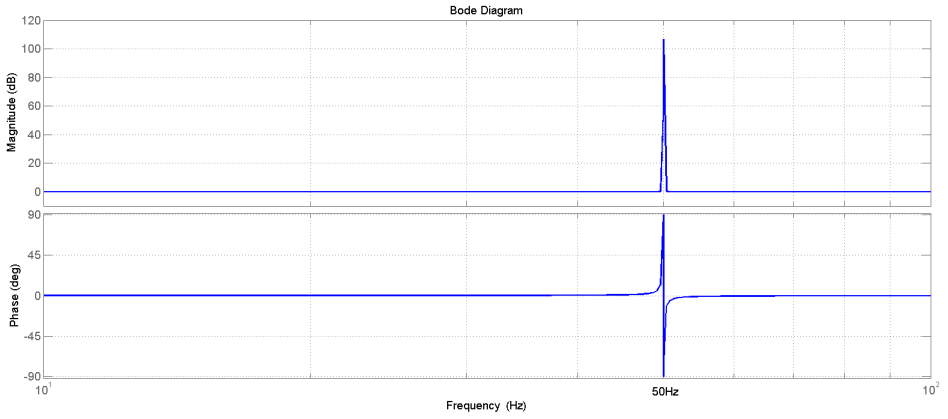

Figure 3.14: Bode plots of PR controller

3.4.4 Improved OSAP Controller and Simulation Research

As stated before, a PR controller has the capability of removing periodic errors, and this feature matches our needs of eliminating the errors in OSAP controllers. By adding the PR controller in the OSAP control systems, now we have the improved OSAP controllers. Their topologies are shown in Fig. 3.15, one is the improved OSAP voltage controller and the other is the OSAP curretn controller.

Simulation researches are also carried out to demonstrate the theories about this improved OSAP controller. Here the improved OSAP voltage control strategy is conducted as an example. The simulation model is exactly the same model in Section 3.2.4. In Section 3.2.4, the inverter is controlled by a single OSAP voltage controller. A one sampling error is found, and this sampling error is introduced by $V_o(k+1)$ replaced by $V_{ref}(k)$. Another error is the tolerance of

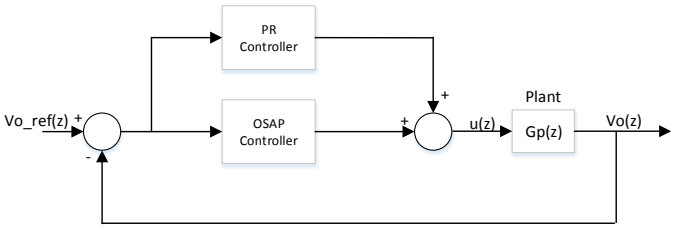

(a)

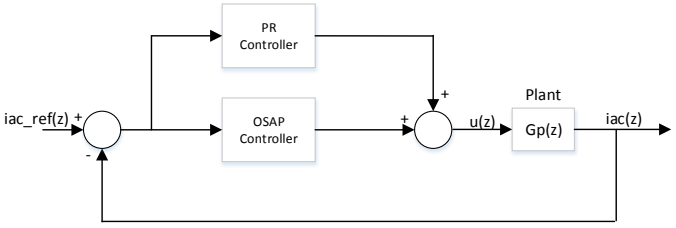

(b)

Figure 3.15: (a) Improved OSAP voltage controller (b) Improved OSAP current controller

the electronic components in reality. This error is shown in Fig. 3.12. The functionality of the PR controller in this improved OSAP controller is expected to eliminate both errors.

The model of this improved OSAP voltage-control inverter is shown in Fig. 3.16 and the value of each component is in Table. 3.3. Here the 10% tolerance of L and C is still included, same as Section 3.4.1.

Table 3.3: Parameters of improved OSAP voltage-control inverter

Output Voltage V_o	$21.2V$	Input Voltage V_{dc}	$60V$
Output Voltage Frequency	$50Hz$	Switching Frequency	$19200Hz$
Inductor L	$7mH$	Capacitor C	$24\mu F$
Resistor R	30Ω	K_p	0.5
K_r	20		

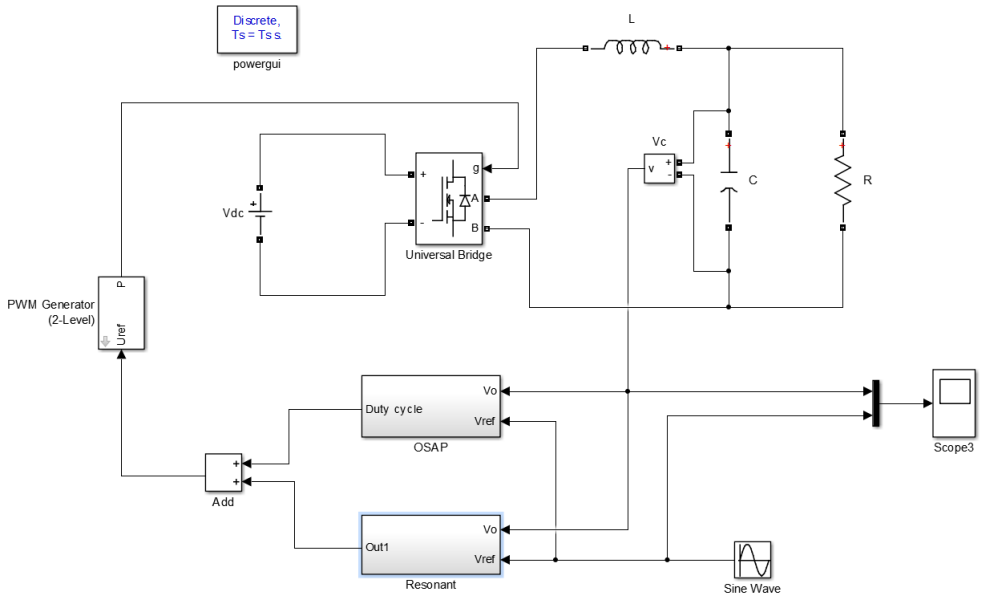

Figure 3.16: Simulation model of OSAP+PR controlled inverter

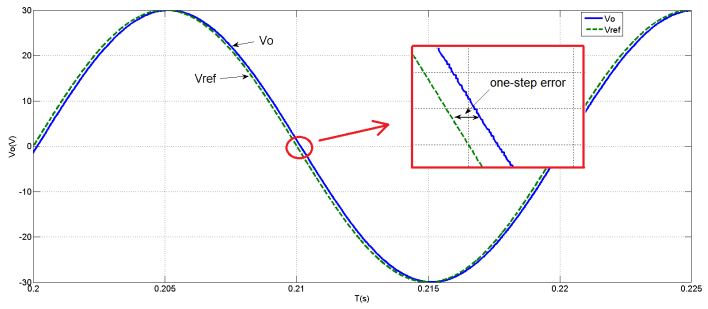

(a)

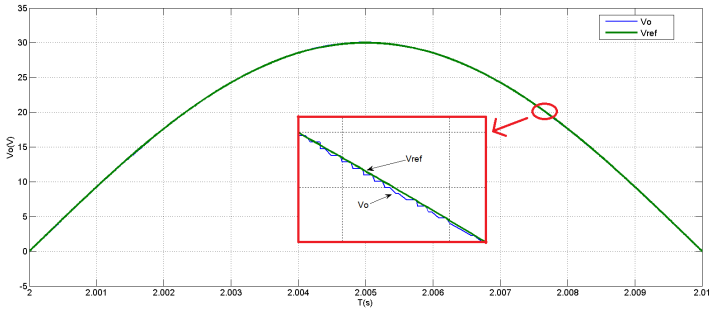

(b)

Figure 3.17: Simulation results of voltage responses (a) OSAP controller (b) OSAP+PR controller

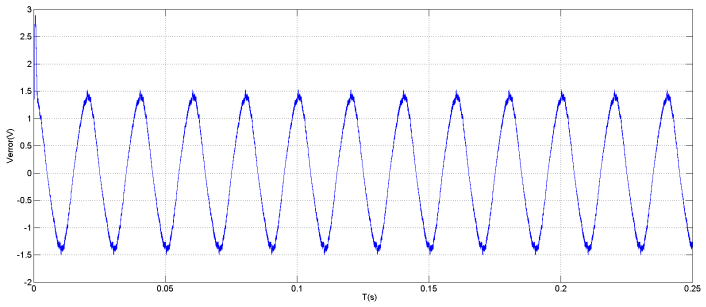

(a)

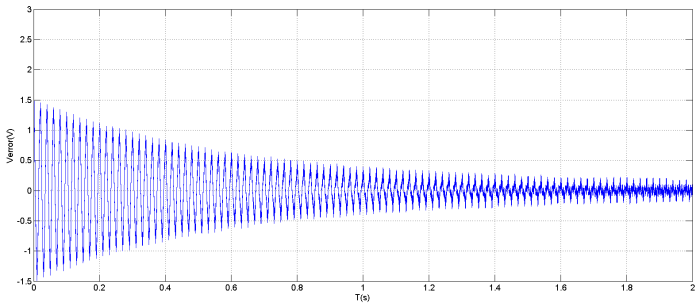

(b)

Figure 3.18: Simulation results of the errors of output voltage (a) OSAP controller (b) OSAP+resonant controller

Based on the error signals shown in Fig. 3.18(b), the resonant controller forces the phase displacement between V_o and V_{ref} and the errors in the voltage magnitude due to component tolerance to zero successfully.

Chapter 4

THE EXPERIMENT

4.1 INTRODUCTION

This chapter introduces the experiment of this project. Two power stages—the DC-DC converter board which conducts the MPPT techniques for solar panels and the DC-AC inverter board which focus on the OSAP control strategies implementation, are introduced separately and experimental results are provided. Afterwards the two stages are combined together to form a solar micro inverter system and experimental results are also given to support the analyses in Chapter 2 and Chapter 3.

The diagram of the experimental circuit is shown in Fig. 4.1, which includes the power stage and the digital control stage. From this diagram, it is clear to see that the whole system can be divided into two main parts—the DC-DC stage and the DC-AC stage. Actually, this experiment is done with help from Texas Instruments—the High Voltage Isolated Solar MPPT Developers Kit and the High Voltage Single Phase Inverter Development Kit are applied as the hardware of this experiment. These two kits are shown in Fig. 4.2. The first MPPT kit contains an interleaved boost convert which is supposed to implement MPPT techniques and the second inverter kit contains a full-bridge inverter which is supposed to implement OSAP control strategies. Both kits are controlled by the high-speed microcontroller TMS320F28035.

Another important piece of equipment applied in this system is the solar panels. Due to limited conditions in the laboratory that simulating a fast changing sun irradiation and the others factors in the environment is not practical, we use a programmable DC power source to simulate the output of a PV panel. The Chroma 62150H-600S DC Power Supply is a programmable DC power supply, which can generate from 600W to 15kW DC power and ensures definable operating voltage or current (Fig. 4.3). In addition, it has a solar array simulator function. This DC source can simulation the output of a solar panel whose open-circuit voltage (V_{oc}) can rise up to 1000V and short-circuit current (I_{sc}) can go up to 25A . Its fast transient response makes this power supply an ideal device for MPPT performance research. Constant voltage is also needed for the experiment of grid-tied inverter as the DC Bus voltage.

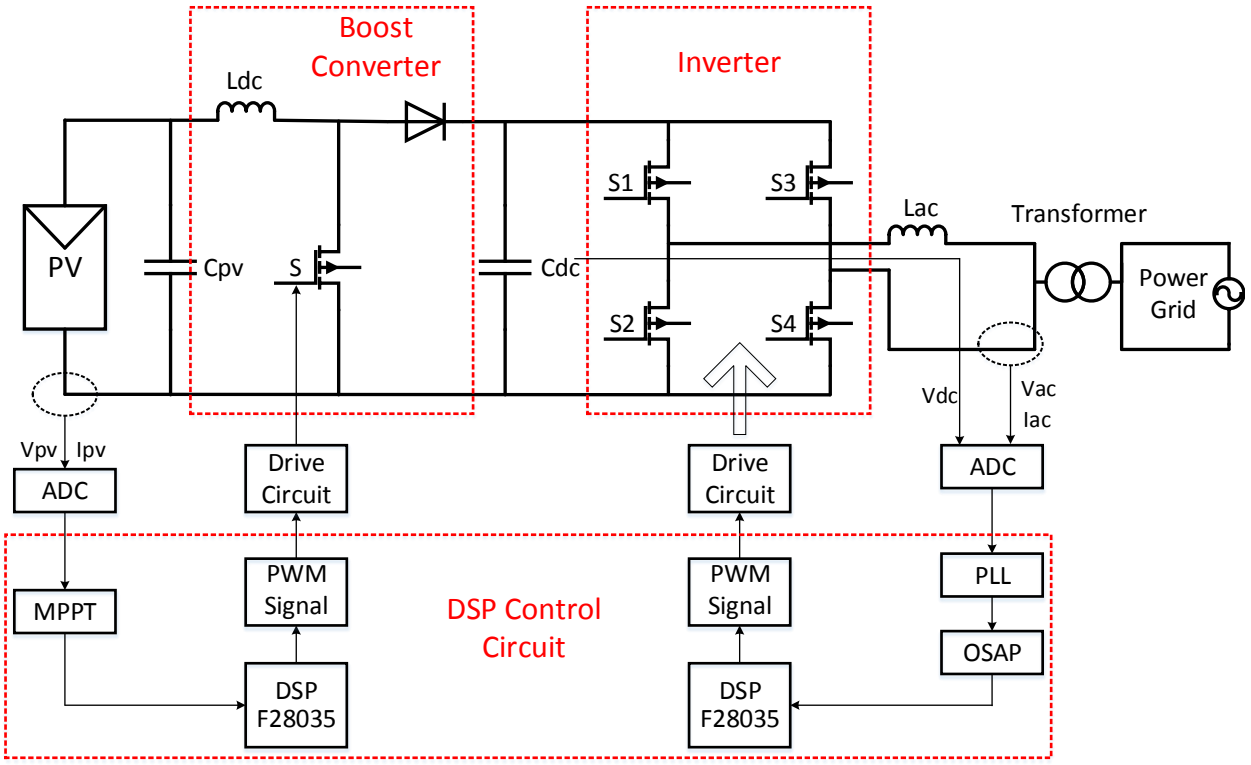

Figure 4.1: Experiment circuit of PV micro-inverter

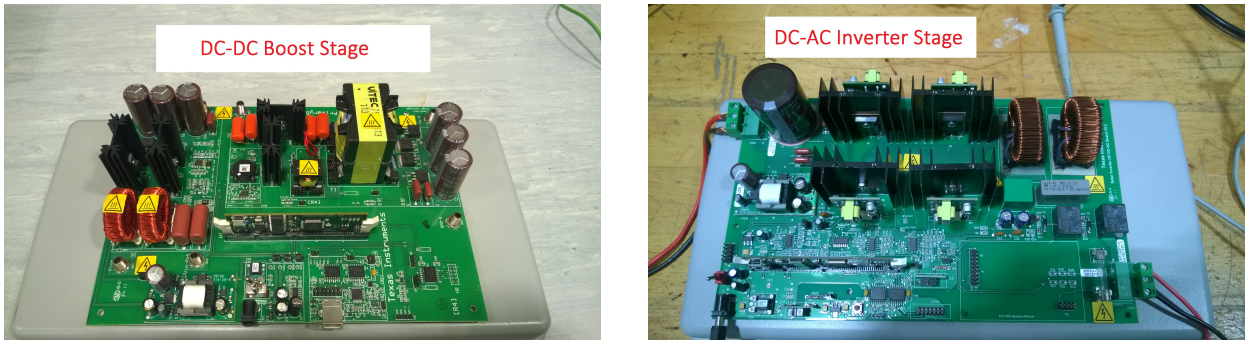

(a) (b)

Figure 4.2: (a) DC-DC boost converter experiment kit (b) DC-AC inverter experiment kit

In the grid-connected inverter experiment, a power grid is needed. In this experiment, the Chroma AC power source Model 61604 is applied to generate constant 220V/50Hz AC voltage. This AC source is shown in Fig. 4.4.

Figure 4.3: Chroma DC power supply 62000H-S

Figure 4.4: Cheoma AC power supply 61604

4.2 IMPLEMENTATION OF DC-DC CONVERTERS

4.2.1 Interleaved Boost Converter

In the DC-DC board, an interleaved boost converter has been applied to implement MPPT strategies. Fig. 4.5 is the circuit diagram. Different from a conventional single-phase boost converter, two-phase interleaved boost converter can be very beneficial for high-demand electrical performance. The advantages that a multiple-phase interleaved boost converter has over a single-phase boost converter are the increased output current, the reduction in input current ripple, the reduction in power losses, the increased efficiency and the reduction in equipment size [51].

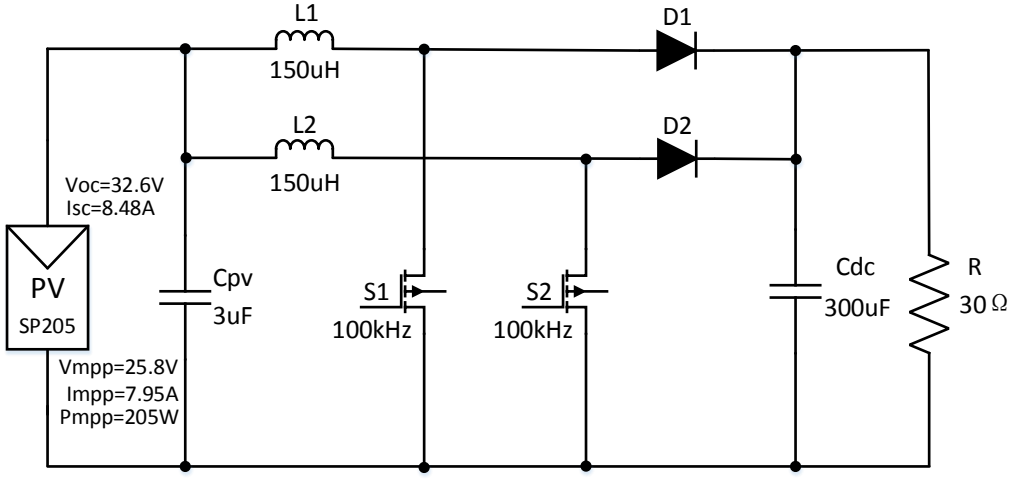

Figure 4.5: Interleaved Boost Converter

The operation signals to drive this two-phase interleaved boost converter are two PWM signals with the same duty cycle and 180 degrees out of phase. The same duty cycle has guaranteed the same current sharing in the two stages. By combining two current ripples in each stage together, the total input current ripple has been reduced. Fig. 4.6 shows the PWM signals (blue one and green one) captured from the micro-controller. They are two 100kHz PWM waveforms with the same duty cycle to drive the boost stage.

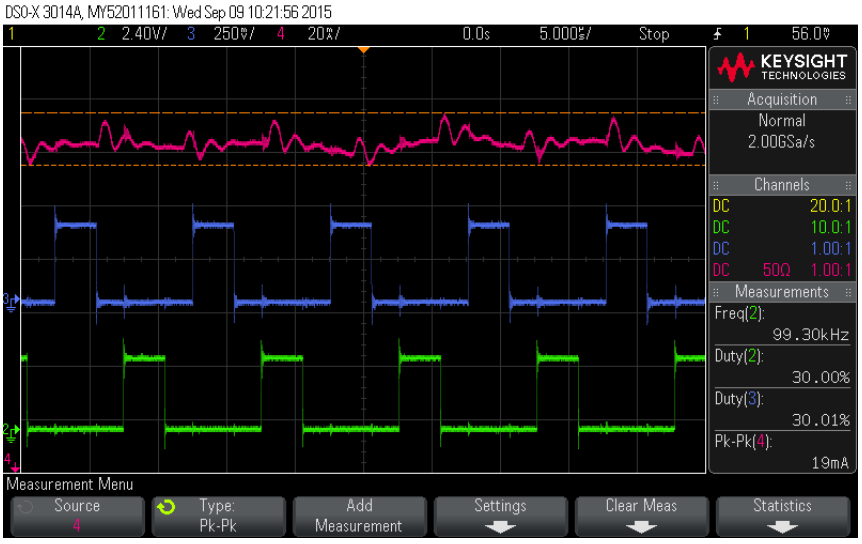

Figure 4.6: PWM signals to drive interleaved boost converter and the input current ripple (a)Channel 2 and 3 are the PWM signals (b) Channel 4 is the input current

Fig. 4.6 also illustrates the reduction in the input current ripple. In this scheme, a 10V DC voltage is applied on this experiment board and the duty cycle is kept at 0.3, the switching frequency is 100kHz. Based on calculation, the input current ripple in a single-phase boost stage with the same inductor and capacitor is about 200mA. In this two-phase stage, this current ripple actually drops to about 19mA, significant current ripple reduction has been achieved.

4.2.2 MPPT Implementation

This section asses the MPPT implementation in this interleaved boost stage. The DC source has been programmed to simulate the solar panel SP205 (this panel has been modelled in Chapter 2), whose open-circuit voltage V_{oc} is 32.8V and MPP voltage V_{mpp} is 25.8V. Two MPPT techniques have been adopted, one is the conventional fixed step-size P&O method and the other is the variable step-size P&O method. Fig. 4.7 is the PV panel voltage captured from the beginning until the MPP is reached. Before starting the system, this PV panel is at open-circuit condition, at this time PV output voltage is 32.8V. Then we start the programme and the PV voltage experiences a significant drop and then raise up again until getting close to the MPP. The fixed

voltage disturbance in 4.7(a) is chosen as 0.01V and the system takes almost 3.5s to get the MPP, significant oscillation is also found around that point afterwards. By contrast, the variable step-size P&O MPPT in 4.7(b) only takes 1.85s to achieve the MPP which is much faster than the fixed step-size MPPT, and the oscillation has been reduced.

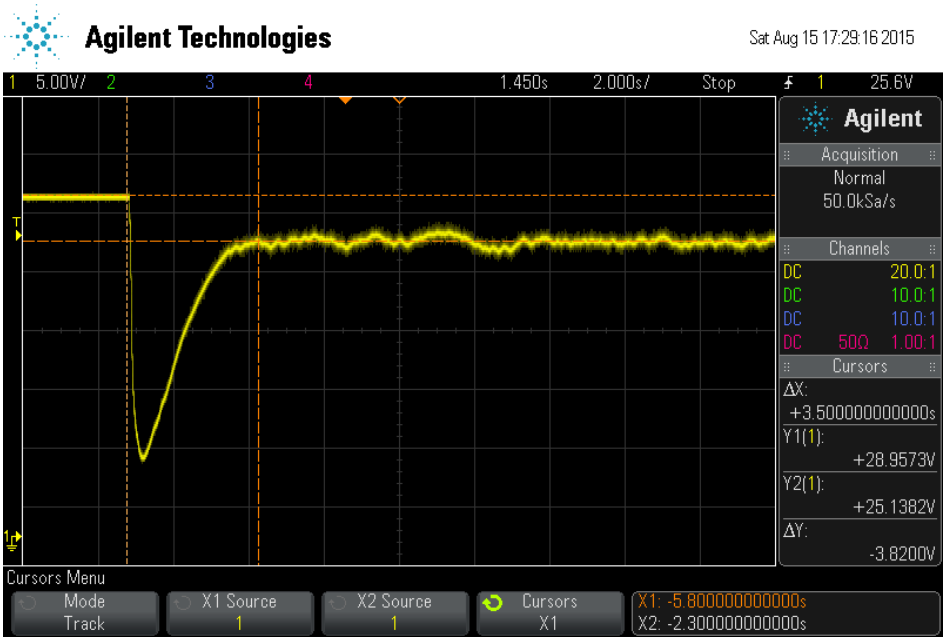

(a)

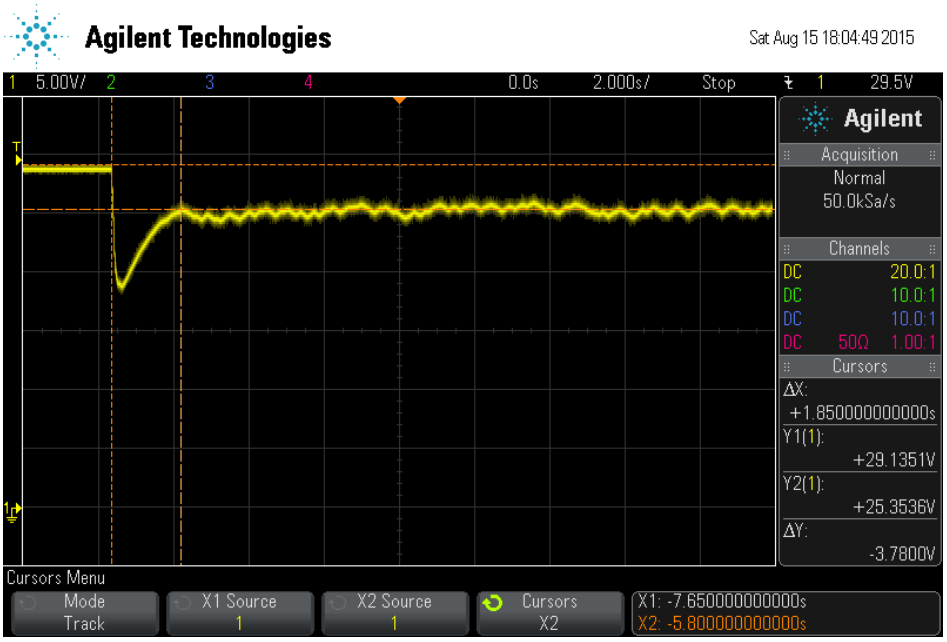

(b)

Figure 4.7: MPPT results (a) Fixed step-size P&O MPPT (b) Variable step-size P&O MPPT

4.3 IMPLEMENTATION OF STAND-ALONE INVERTER

4.3.1 Full-Bridge Inverter and LC Filter Design

In the DC-AC board, a full-bridge inverter has been used to perform the OSAP control strategies. The circuit diagram of the board is shown in Fig. 4.8.

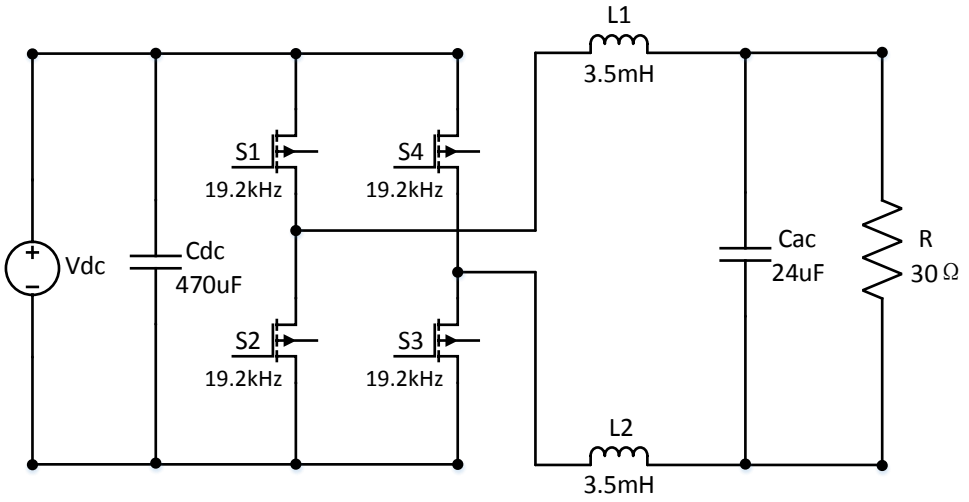

Figure 4.8: Full-bridge Inverter

In this inverter, a LC low-pass filter has been applied. The transfer function between the switched input voltage pulse V_{in} and the output AC voltage V_{ac} through this LC filter is:

$$V_{ac}(s) = \frac{R}{RLC \cdot s^2 + Ls + R} \cdot V_{in}(s) \tag{4.1}$$

Now we fix the value of the inductor and resistor to be constant, which is $L = 7\text{mH}$ and $R = 30\Omega$, and chose four different values for the capacitor, which is $C_1 = 1\mu\text{F}$, $C_2 = 24\mu\text{F}$, $C_3 = 133\mu\text{F}$ and $C_4 = 220\mu\text{F}$. The bode diagram of the transfer function of the LC filter is shown in Fig. 4.9. There exists a resonant frequency $\omega = \sqrt{\frac{1}{LC}}$, which provides the maximum gain. From Fig. 4.9 it is apparent that with the constant L and R, the larger capacitance, the lower the resonant frequency. However, when the LC filter is designed, only a filter is desired rather than an amplifier. The resonant frequency should not be too close to the operating frequency (i.e. 50Hz). In addition, the voltage gain due to the filter will have a influence on the control loop and affect the inverter design.

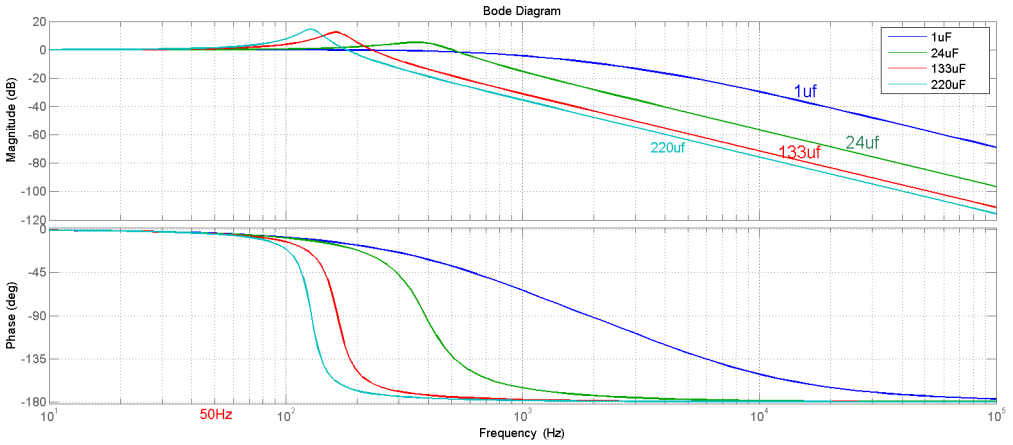

Figure 4.9: Bode Diagram of LC filter with different capacitance

4.3.2 OSAP voltage controller

Experimental results of the OSAP voltage-control inverter with different capacitors are shown in Fig. 4.10. The input DC voltage V_{dc} is 60V and the controlled output AC voltage V_{ac} is 30V (peak value). Two capacitors are applied and the OSAP controller is updated with different capacitor values. Fig. 4.10(a) and 4.10(b) are the results of a 24μF capacitor and Fig. 4.10(c) is for a 133μF capacitor. Obviously large distortion is found with the 133μF capacitor. By contrast, even the 24μF capacitor provides less distortion, the peak value the of output voltage is just 20V, which is far away from 30V. Fig. 4.10(b) is captured from the microcontroller, where the yellow line is the reference signal and the green line is the feedback signal. A significant error exists between them, which demonstrates single OSAP controller can not provide perfect control results. In addition, some offset is found in Fig. 4.10(a), this is caused by the inaccuracy of the ADC (analogue-digital conversion) module in the microcontroller, and it is fixed in the next experiment by adding an offset value for compensation in the microcontroller.

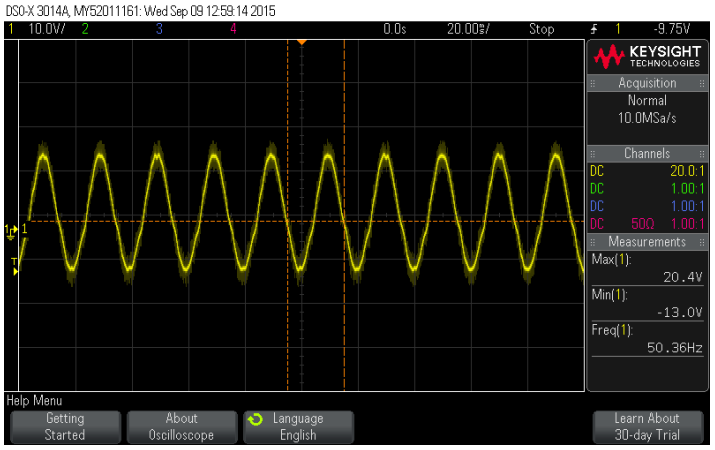

(a)

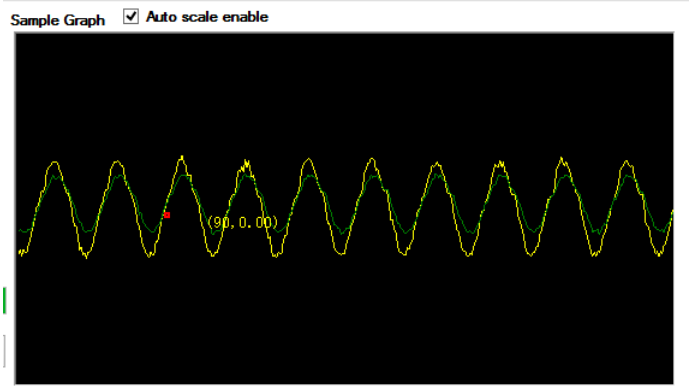

(b)

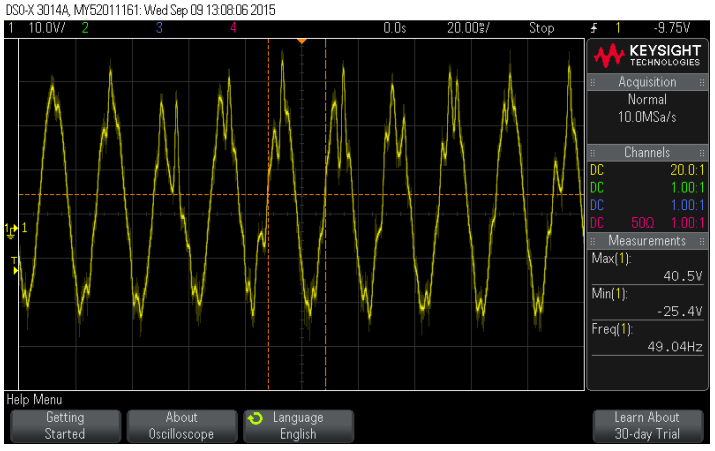

(c)

Figure 4.10: OSAP voltage-control inverter results (a) output voltage with 24μF capacitor (b) reference signal and the feedback signal with 24μF capacitor (c) output voltage with 133μF capacitor

4.3.3 OSAP+PR Voltage Controller

In order to compensate for the practical shortcomings of OSAP control strategies, a resonant controller is added with the OSAP controller to form the improved OSAP controller in Chapter 3. This improved OSAP controller can not only correct the errors in output voltage due to component tolerance, but also eliminate the steady-state errors introduced by the deadbeat control strategy. Fig. 4.11 is the controlled AC output voltage for this stand-alone inverter with improved OSAP controller. All the component values are the same in Section 4.3.2 and AC side capacitor is 24μF. The output voltage matches the reference value, which is 30V at the peak and THD is 4.70%. This has shown that the improved OSAP controller is better than a single OSAP controller.

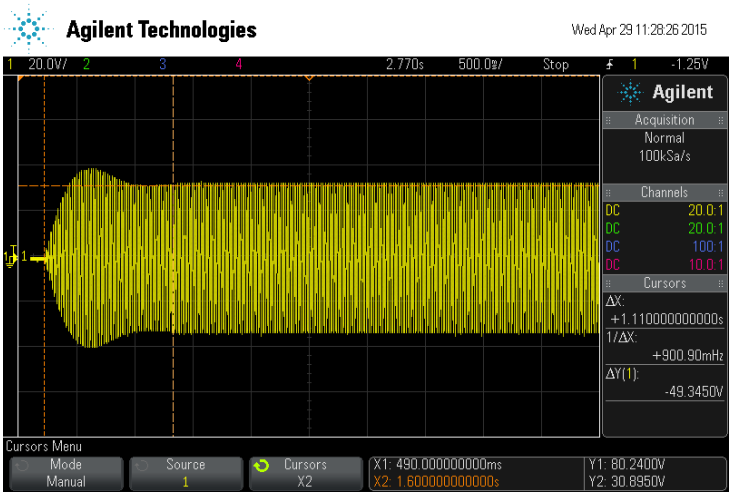

(a)

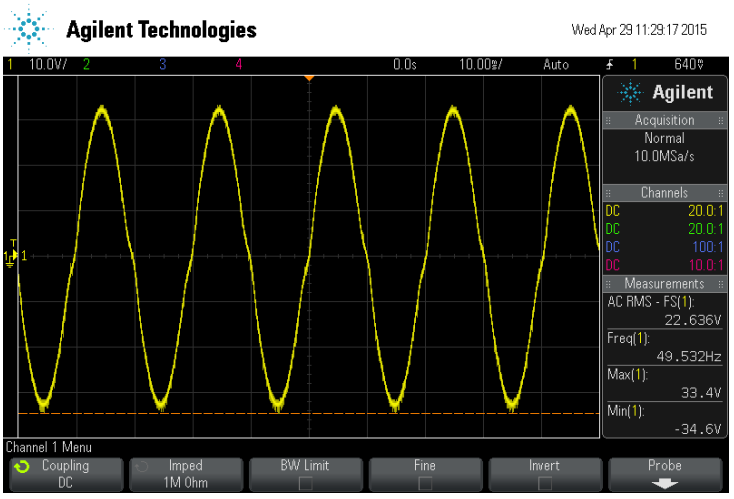

(b)

Figure 4.11: Improved OSAP voltage-control inverter (a) taking 1.6s to stabilize (b) output voltage in steady state

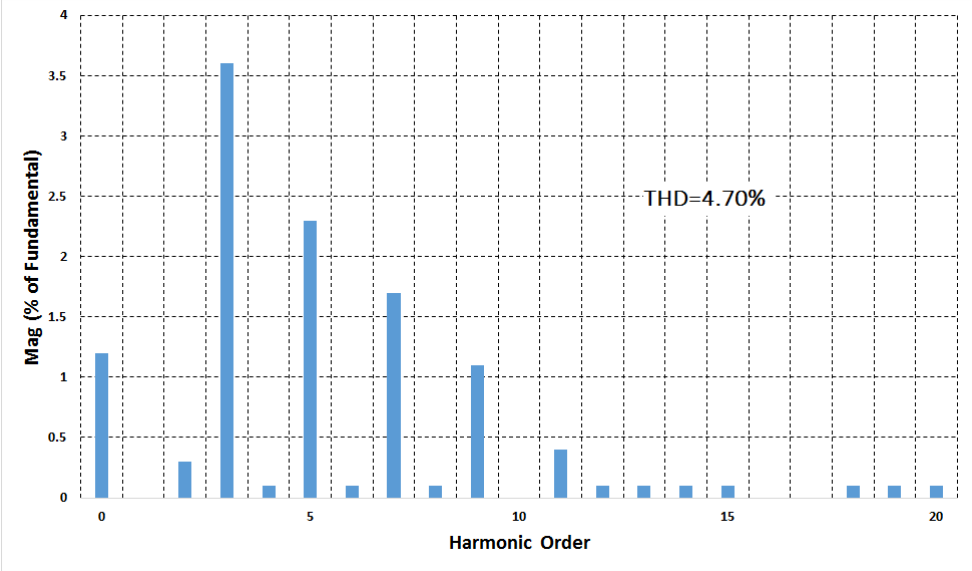

Figure 4.12: THD of the output voltage (the value of the fundamental frequency is not shown in this graph)

4.4 IMPLEMENTATION OF GRID-TIED SOLAR MICRO-INVERTER

This section illustrates the complete experimental results of a single-phase photovoltaic grid-tied micro inverter. The whole system circuit is shown in Fig. 4.13. As mentioned before, a Chroma AC power supply 61600 is applied to simulate the power grid. Since this power source does not have the ability to absorb any power, the 85Ω resistive load is always utilized. The isolation transformer is placed between the inverter and AC source for safety reasons. The 24μF capacitor on the AC side is also removed and the 7mH inductor is the filter for this inverter.

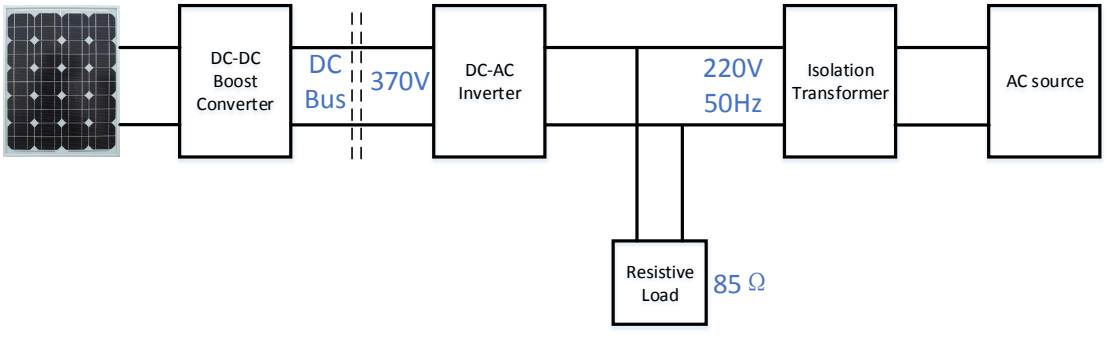

Figure 4.13: Photovoltaic Grid-tied Micro Inverter

Variable step-size P&O MPPT is applied to control the DC-DC converter and the improved OSAP current controller which is designed in Section 3.4.4 is used to control the grid-connected inverter. The solar panel is still the SP205 solar panel, as discussed in previous chapters, and its output power is 205W at the MPP. DC Bus voltage is maintained at 370V by the inverter.

Experimental results are shown below.

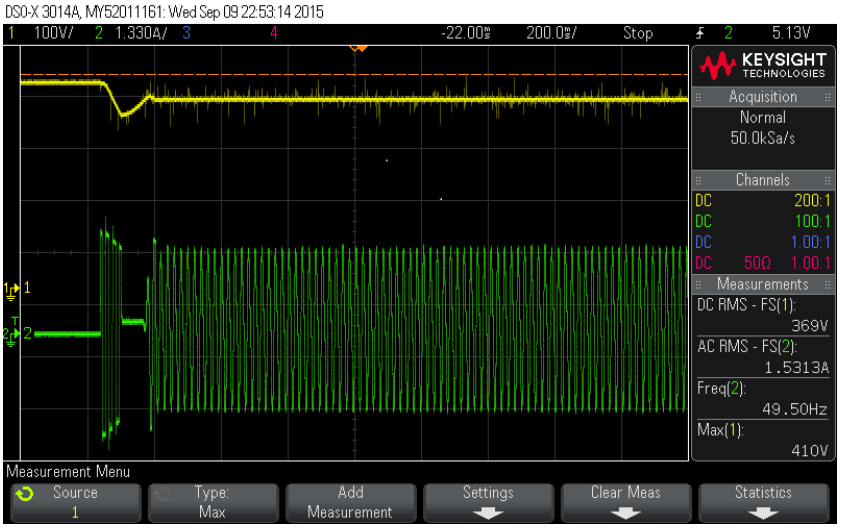

Figure 4.14: DC Bus voltage and AC output current

Fig. 4.14 shows the response of the DC Bus voltage (yellow) and AC output current (green) from the start of system operation until stable conditions. Before the start of inverter, the MPPT is already running, so the DC Bus voltage is 410V at the beginning and AC output current is 0. Then, the current-controlled inverter begin to operate. The system takes about 100ms to get stabilised and DC Bus voltage drops to 369V and remains constant. The output current is 1.53A and the inverter output power is 199W, which matches the solar panel output power 205W (practical power losses needs to be taken into consideration).

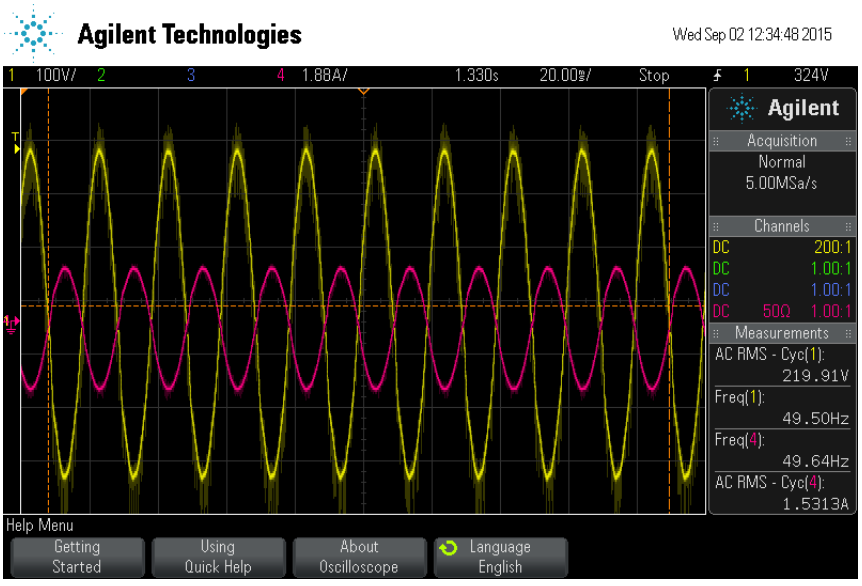

Figure 4.15: Grid voltage and AC output current

Fig. 4.15 is the AC voltage (yellow) and inverter output current (pink). Inverter output current

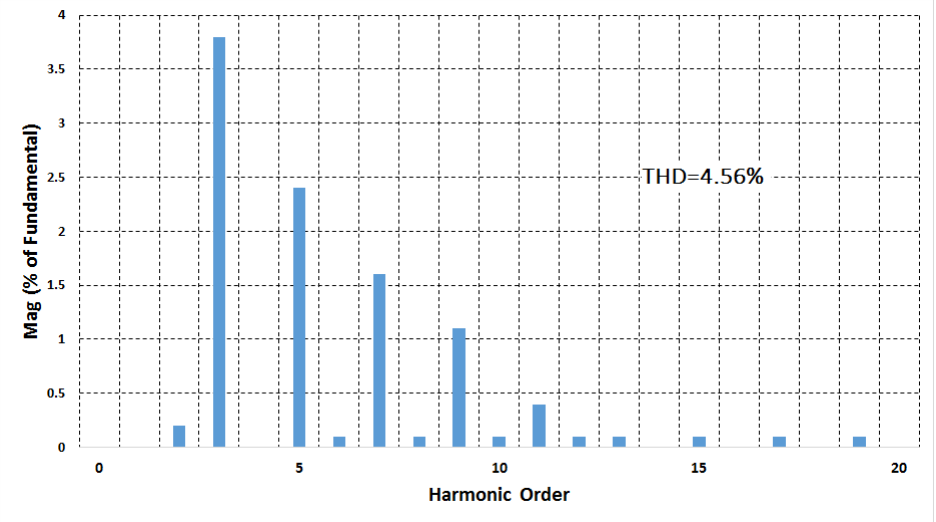

Figure 4.16: THD of output current (the value of the fundamental frequency is not shown in this graph)

and grid voltage are 180 degrees out of phase. Fig. 4.16 shows the THD of the output current, which is 4.56%.

A irradiation change on the solar panel has also been simulated on the DC source to show the transient response of this solar system. Fig. 4.17 is the transient response of DC Bus voltage (yellow) and AC output current during shading problems. In this shading problem, the panel output power drops from 205W to 120W. Oscillation is found in both curves, but the system gets stable after nearly 500ms. The DC Bus voltage is still 370V and AC output current drops to 1.098A due to the reduction of solar panel output power.

This result has shown that the inverter works very well with good power quality, good efficiency and a fast transient response. This demonstrates that the inverter control design is practical and has good performance.

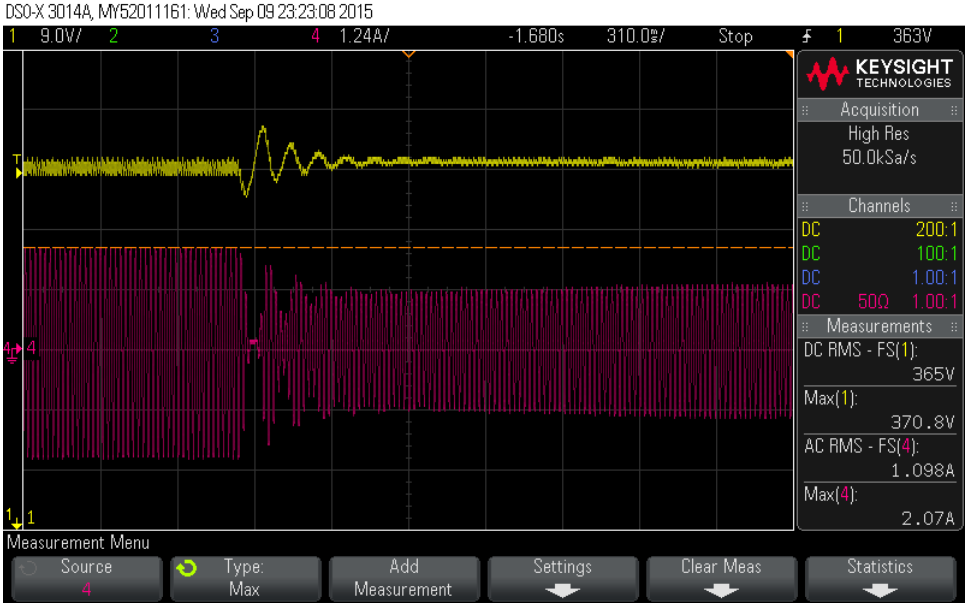

Figure 4.17: Transient response of DC Bus voltage and AC output current under solar panel irradiation changes

Chapter 5

CONCLUSIONS

5.1 CONCLUSIONS

The main subject of this project is to develop an advanced control strategy for a solar micro-inverter to optimize the system effectiveness. Development of theory and experiment have been conducted on solar cell maximum power point tracking strategies and grid-tied inverter control strategies. The experiment results have demonstrated the theory and goals have been achieved. The main contributions of this thesis are listed below:

1. The mathematical model and simulation model of solar cells have been built. Simulation has been conducted for the analysis of the output characteristics of solar cells. Typical MPPT strategies have been introduced. Evaluations of Constant Voltage MPPT, P&O MPPT and INC MPPT are provided and they are compared with each other. Taking the P&O MPPT as an example, the disadvantages of conventional fixed step-size MPPT strategies are also analysed. An advanced variable step-size P&O MPPT algorithm is then proposed to overcome these shortcomings. Simulation results have been provided to demonstrate the advantages of this advanced MPPT strategy over the conventional one, which include high accuracy, short response time and no oscillation at the MPP.

2. The model of a full-bridge inverter has been built and analysed. Two working states of this inverter are proposed: stand-alone inverter and grid-tied inverter. A deadbeat control strategy, named the one-sampling-ahead-preview (OSAP), is proposed for the inverter, which include the OSAP voltage-control strategies for the stand-alone inverter and the OSAP current-control strategies for the grid-tied inverter. Simulations have been conducted for both inverters and simulation results demonstrate the theory. The disadvantages of this single OSAP controller are analysed—this deadbeat controller brings a deadbeat response to the output and OSAP controller relies on the inverter having accurate values for its components. In order to compensate these disadvantages, the resonant controller which is based on the Internal Model theory is introduced. With the combination of a resonant controller, an improved OSAP controller is then proposed. Simulation results are shown to support that this improved OSAP controller

can eliminate the deadbeat errors and variable values of electronic components can be tolerated and bring no uncertainties to the control loop.

3. Based on the theory and simulations, experiments on a single-phase photovoltaic micro-inverter have been conducted. The whole system has been divided into two separate parts for experiment— the DC-DC boost converter and DC-AC single-phase inverter. The controllers in both parts are implemented in a high-speed microcontroller TMS320F28035. In the boost converter, an interleaved boost converter topology is adopted, this two-phase topology has the advantages over a single-phase boost converter, such as the reduction of input current ripple and the reduction in power losses. Experimental results are provided to compare a conventional fixed step-size P&O MPPT with a variable step-size P&O MPPT. With the same circuit and conditions, the variable step-size MPPT technique has demonstrated its advantages over the conventional one. Then the experiments have been performed on the DC-AC inverter. One experiment is for a stand-alone inverter, where the OSAP voltage-control strategy is applied. Comparison between a single OSAP controller and an improved OSAP controller is provided, which demonstrates that single OSAP controllers are not suitable for the practical situation, and the improved OSAP controllers can achieve the control goals. Finally, the DC-DC part and DC-AC part are combined together to form the grid-connected inverter system. Experiment results are also given.

5.2 RESEARCH PERSPECTIVES

Although many aspects have been documented in this thesis for advanced single-phase solar micro-inverter technologies, there are still a lot of possibilities for technology improvement. Some issues are still existing in this PV system for further investigations, which are listed below:

1. For the variable step-size MPPT, both the simulation and experiment are done in a constant environment, i.e. constant irradiation and temperature. The responses of this MPPT technique under a continuously variable environment, especially the rapidly changing environmental conditions, are not considered in this research yet. Actually, some MPPT techniques can not work well in the low-irradiation conditions and fast-changing environment sometimes can confuse the controller to determine the step-size of perturbation.

2. In the inverter design, the problem of harmonics has not been taken into consideration. An simple low-pass LC or L filter is not enough for the requirement of low THD and harmonic reduction. Actually, the THD is about 4.56% in the grid-tied inverter experiment, which meets the minimum standards for grid-connected inverters but is still relatively high. In further researches, reduction of harmonics have to be conducted both at the control level and hardware level. Papers suggest repetitive controllers and LCL filters could be the possible solutions.

3. The problem of islanding is not considered. Islanding comes up with the distributed generation and is quite dangerous. The detection of the islanding is important for both the power grid and the connected micro grid. Several techniques are now available for the micro grid system to detect an islanding situation and cut itself off from the utility immediately when islanding happens.

Besides those interesting topics, the development and implementation of this grid-tied solar inverter are still far away from finalization. PV micro-inverters and distributed generation are still new concepts for the industry, which need further development and deeper understanding. But with the amazing innovations in the technology, we believe the application of these new concepts has a bright future.

REFERENCES

[1] (2010) A statement of the problem in capsule form. [Online]. Available: http://planetforlife.com/

[2] J. Arrillaga and P. S. Bodger, *Gathering Renewable Energy in Electrical Networks*, 1st ed. EPECntre, 2009.

[3] F. R. R. Eduardo F. Camacho, Manuel Berenguel and D. martínez, *Control of Solar Energy Systems.* Springer, 2012.

[4] F. Kreith, *Principles of Sustainable Energy Systems*, 2nd ed. CRC Press, 2013.

[5] Energy Efficiency and Conservation Authority, "Power from the people: a guide to micro-generation," Dec 2010.

[6] (2015) Our renewable energy resources. [Online]. Available: http://www.eeca.govt.nz/efficient-and-renewable-energy/renewable-energy

[7] (2013) The price of wind power in new zealand. [Online]. Available: http://policyprojects.ac.nz/edwardochoa/background-information/renewable-energy-in-new-zealand/

[8] (2015) Photovoltaics. [Online]. Available: https://en.wikipedia.org/wiki/Photovoltaics

[9] (2015) String inverters vs. microinverters vs. power optimizers. [Online]. Available: https://www.energysage.com/solar/101/string-inverters-microinverters-power-optimizers

[10] R. H. Lasseter, "Microgrids and distributed generation," *Journal of Energy Engineering*, vol. 133, pp. 144–149, 2007.

[11] A. Luque and S. Hegedus, *Handbook of Photovoltaic Science and Engineering.* Wiley, 2011.

[12] A. R. Jha, *Soalr Cell Technology and Applications.* CRC Press, 2009.

[13] M. C. D. Piazza and G. Vitale, *Photovoltaic Sources: Modeling and Emulation.* Springer, 2012.

[14] T. Saga, "Advances in crystalline silicon solar cell technology for industrial mass production," *NPG ASIA MATERIALS*, vol. 2, 2010.

[15] V. S. Ryaben'kii and S. V. Tsynkov, *A Theoretical Introduction to Numerical Analysis*. Chapman and Hall/CRC, 2006.

[16] W. Z. M. W. Y. S. Jianhui Su, Shijie Yu and H. He, "Investigation on engineering analytical model of silicon solar cells," *Acta Energiae Solaris Sinica*, vol. 22, no. 4, pp. 409–412, 2001.

[17] M. H. M. Ali Reza Reisi and S. Jamasb, "Classification and comparison of maximum power point tracking techniques for photovoltaic system: A review," *Renewable and Sustainable Energy Reviews*, vol. 19, pp. 433–443, 2013.

[18] L. G. Aleck W. Leedy and K. A. Aganah, "A constant voltage mppt method for a solar power boost converter with dc motor load," in *Southeastcon, 2012 Proceedings of IEEE*. Orlando: IEEE, 2012, pp. 1–6.

[19] T. Esram and P. L. Chapman, "Comparison of photovoltaic array maximum power point tracking techniques," *IEEE TRANSACTION ON ENERGY CONVERSION*, vol. 22, no. 2, pp. 439–449, 2007.

[20] B. Bekker and H. J. Beukes, "Finding an optimal pv panel maximum power point tracking method," in *Proc. 7th AFRICON*, Africa, 2004, pp. 1125–1129.

[21] V. A. Sachin Jain, "A new algorithm for rapid tracjing of approximate maximum power point in photovoltaic systems," *Power Electronics Letters*, vol. 2, no. 1, pp. 16–19, 2004.

[22] S. W. Ratna Ika Putri and M. Rifa'i, "Maximum power point tracking for photovoltaic using incremental conductance method," in *2nd International Conference on Sustainable Energy Engineering and Application*. Indonesia: ICSEEA, 2014, pp. 22–30.

[23] (2009) Maximum power point tracking. [Online]. Available: http://www.ni.com/white-paper/8106/en/

[24] J. R. G. Vinodhkumar and M. Sasikumar, "Perfoemance enhancement in pv system using intelligent controller based mppt controller," *IOSR Journal of Engineering*, vol. 2, no. 2, pp. 284–287, 2012.

[25] F. L. B. L. Fangrui Liu, Shanxu Duan and Y. Kang, "A variable step size inc mppt method for pv system," *IEEE Transaction on Industrial Electronics*, vol. 55, no. 7.

[26] A. Papacasoliou, "Current control of a voltage source inverter connected to the grid via lcl filter," *Transactions on Power apparatus and systems*, vol. 89, no. 1, pp. 125–130, 1970.

[27] S. Narendiram, "Grid tie inverter and mppt- a review," in *2013 International Conference on Circuits, Power and Computing Technologies*. Nagercoil: IEEE, 2013, pp. 20–21.

[28] R. T. Mihai Ciobotaru and F. Blaabjerg, "Control of single-phase pv inverter," in *Power Electronics and Application, 2005 European Conference*, Dresden, 2005, pp. 1–10.

[29] M. M. Saeed Go1estan and J. M. Guerrero, "Second order generalized integrator based reference current generation method for single-phase shunt active power filters under adverse grid conditions," in *Power Electronics, Drive Systems and Technologies Conference (PEDSTC), 2013 4th*, Tehran, 2013, pp. 510–517.

[30] C. N.-M. Ho and H. S.-H. Chung, "Constant-frequency hysteresis current control of grid-connected vsiwithout bandwidth control," *Power Electronics*, vol. 24, pp. 2484–2495, 2009.

[31] K. Vladimr, "Deadbeat control, pole placement, and lq regulation," *Kybernetika*, vol. 35, pp. 681–692, 1999.

[32] K. Ogata, *Discrete-Time Control Systems*, 2nd ed. Prentice Hall, 1994.

[33] M. R. I. F. katiraei and P. W. Lehn, "Micro-grid autonomous operation during and subsequent to islanding process," *IEEE TRANSACTION ON POWER DELIVERY*, vol. 20, no. 1, pp. 248–257, 2005.

[34] H. Patel and V. Agarwal, "Control of a stand-alone inverter-based distributed generation source for voltage regulation and harmonic compensation," *IEEE TRANSACTION ON POWER DELIVERY*, vol. 23, no. 2, pp. 1113–1120, 2008.

[35] K. P.GOKHALE, "Dead beat micoprocessor control of pwm inverter for sinusoidal output waveform synthesis," *IEEE TRANSACTION ON INDUSTRY APPLICATIONS*, vol. IA-23, no. 5, 1987.

[36] D. Rowell, *Time-Domain Solution of LTI State Equation*. MIT Department of Mechnical Engineering: Class Handout, 2002.

[37] K. Zhou, "Periodic errors elimination in cvcf pwm dc/ac converter systems: Repetitive control approach," in *IEEE Proceedings-Control Theory Application*, vol. 147, no. 6.

[38] T. H. ATUSO KAWAMURA and R. G. HOFT, "Deadbeat controlled pwm inverter with parameter estimation using only voltage sensor," *IEEE Transaction on Industrial Electronics*, vol. 3, no. 2.

[39] E. Mircea and S. Mohammad, *Handbook of Electrical Power System Dynamics:Modeling, Stability, and Control*. Wiley, 2013.

[40] K. Zhou, "Digital repetitve controlled three-phase pwm rectifier," *IEEE TRANSACTION ON POWER ELECTRONICS*, vol. 18, no. 1.

[41] T. Green and M. Prodanovi, "Control of inverter-based micro-grids," *Electric Power Systems Research*, vol. 77, no. 9, Jul 2007.

[42] B. Kirby and E. Hirst, "Ancillary service details: Voltage control," Dec 1997.

[43] (2015) Inverters, controlled rectifiers, and the scr. [Online]. Available: http://powercircuits.net/inverters-controlled-rectifiers-scr/

[44] U. A. Ahmet M. Hava and V. V. Aban, "A dc bus capacitor design method for various inverter application," in *Energy Conversion Congress and Exposition,2012 IEEE*, Raleign, NC, 2012, pp. 4592–4599.

[45] R. Teodorescu, "Proportional-resonant controllers. a new breed of controllers suitable for grid-connected voltage-source converters," *Journal of Electrical Engineering*, vol. 3, pp. 9–14, 2004.

[46] M. Gupta, "Robust Repetitive Model Predictive Control For Systems With Uncertain Period-Time," Ph.D. dissertation, Georgia Institute of Technology, Atlanta, USA, 2004.

[47] S. N. J. H. Lee and K. S. Lee, "A model-based predictive control approach to repetitve control of continuous process with periodic operations," *Journal of Process Control*, vol. 11, pp. 195–207, 2001.

[48] P. Y. Li, "Internal model principle and repetitve control," University Lecture, Apr 2006.

[49] M. T. Tham, "Internal model control," University Lecture, 2002.

[50] A. T. S. Rafael da Silveira Castro, Jeferson Vieria Flores and L. F. A. Pereira, "A comparative analysis of repetitive and resonant controllers to a servo-vision ball and plate system," in *Preprints of the 19th IFAC World Congress*, South Africa, 2014, pp. 1120–1125.

[51] S. M. James Scofield and B. Jordan, "Studies of interleaved dc-dc boost converters with coupled inductors," http://www.dtic.mil/dtic/tr/fulltext/u2/a542736.pdf, Apr 2011.